The Effect of Receiver Nonlinearity and Nonlinearity Induced Interference on the Performance of Amplitude Modulated Signals

Natalie Cary Moore

Thesis submitted to the Faculty of the

Virginia Polytechnic Institute and State University

in partial fulfillment of the requirements for the degree of

Master of Science

in

Electrical Engineering

Jeffrey H. Reed, Chair

William C. Headley

A. A. (Louis) Beex

July 13, 2018

Blacksburg, Virginia

Keywords: Receiver nonlinearity, probability density function, bit error rate, symbol error rate, PAM modulation, QAM modulation, interference, blocking signals

The Effect of Receiver Nonlinearity and Nonlinearity Induced Interference on the Performance of Amplitude Modulated Signals

Natalie Cary Moore

ACADEMIC ABSTRACT

All wireless receivers have some degree of nonlinearity that can negatively impact performance. Two major effects from this nonlinearity are power compression, which leads to amplitude and phase distortions in the received signal, and desensitization caused by a high powered interfering signal at an adjacent channel. As the RF spectrum becomes more crowded, the interference caused by these adjacent signals will become a more significant problem for receiver design. Therefore, having bit and symbol error rate expressions that take the receiver nonlinearity into account will allow for determining the linearity requirements of a receiver. This thesis examines the modeling of the probability density functions of M-PAM and M-QAM signals through an AWGN channel taking into account the impact of receiver nonlinearity. A change of variables technique is used to provide a relationship between the pdf of these signals with a linear receiver and the pdf with a nonlinear receiver. Additionally, theoretical bit and symbol error rates are derived from the pdf expressions. Finally, this approach is extended by deriving pdf and error rate expressions for these signals when nearby blocking signals cause desensitization of the signal of interest. Matlab simulation shows that the derived expressions for a nonlinear receiver have the same accuracy as the accepted expressions for linear receivers.

The Effect of Receiver Nonlinearity and Nonlinearity Induced Interference on the Performance of Amplitude Modulated Signals

Natalie Cary Moore

GENERAL AUDIENCE ABSTRACT

All wireless receivers have some amount of nonlinearity that can distort a received signal and impact performance. For amplitude modulated signals, the power compression caused by the nonlinear receiver will cause distortions in the amplitude and phase of the received signal. Additionally, a high powered interfering signal at a close frequency can decrease the gain and distort the received signal. This thesis examines how the probability density of an amplitude modulated signal with a nonlinear receiver can be modeled for both of these situations. These theoretical probability density functions are used to derive theoretical error rate expressions for the signals both with and without the adjacent channel interference. Simulations in Matlab show that the accuracy of these derived expressions is similar to the accuracies of the linear receiver expressions. These derived expressions will be able to remove the need for time consuming simulation when designing receivers for wireless systems.

Contents

1 Introduction and Motivation **1**

1.1 Thesis Outline and Research Contributions 6

2 Receiver Nonlinearity **7**

2.1 Characteristics of an RF Front End 7

2.2 RF Front End Modeling - Polynomial Model 8

2.3 Effects of a Nonlinear Receiver 10

2.3.1 Power Compression 10

2.3.2 Harmonic Distortion 11

2.3.3 Intermodulation 12

2.3.4 Cross Modulation 15

2.4 Summary 16

3 Modeling the Probability Density Functions of Amplitude Modulated Signals with Receiver Nonlinearity **17**

3.1 M-PAM and M-QAM Modulation 18

3.2 Signal Constellation Distortion Due to Receiver Nonlinearity 19

3.3 Determining Probability Density Function Expressions for Receivers with Nonlinearity in an AWGN Channel 19

3.3.1 Using a Change of Variables to Derive the PDF for a Nonlinear Receiver 21

3.3.2 Probability Density Functions of M-PAM and M-QAM Signals with a Nonlinear Receiver 23

3.3.2.1 Modeling the PDF of M-PAM Signals with a Nonlinear Receiver 23

3.3.2.2 Modeling the PDF of M-QAM Signals with a Nonlinear Receiver 25

3.4 Comparison of Theoretical PDF Expressions with Simulated PDF Expressions 26

3.4.1 Simulated and Theoretical Probability Density Functions 26

3.4.2 Accuracy of Theoretical Results 34

3.5 Summary 41

4 Modeling the Probability Density Functions of M-PAM and M-QAM Signals with Nonlinear Receivers in the Presence of Interference 43

4.1 The Effect of a Tone Blocker on the Probability Density Function 44

4.2 The Effect of an M-PAM Modulated Blocker on the Probability Density Function 47

4.3 The Effect of an M-QAM Modulated Blocker on the Probability Density Function . . . 49

4.4 Results . . . 50

4.4.1 Tone Blocker PDF Accuracy . . . 51

4.4.2 M-PAM Blocker PDF Accuracy . . . 54

4.4.3 M-QAM Blocker PDF Accuracy . . . 57

4.5 Summary . . . 58

5 The Bit and Symbol Error Rates for M-PAM and M-QAM Signals with Nonlinear Receivers with and without the Presence of Interference 60

5.1 Bit and Symbol Error Rate Expressions for M-PAM and M-QAM Signals with Receiver Nonlinearity . . . 61

5.1.1 Bit and Symbol Error Rates for M-PAM . . . 61

5.1.2 Bit and Symbol Error Rates for M-QAM . . . 63

5.2 Bit and Symbol Error Rate Expressions in the Presence of Interference . . . 65

5.2.1 Tone Interference . . . 66

5.2.2 M-PAM Interference . . . 66

5.2.3 M-QAM Interference . . . 67

5.3 Comparison of Theoretical Expressions with Simulated Results . . . 68

5.3.1 Receiver Nonlinearity with No Interference 68

5.3.2 Receiver Nonlinearity with Interference 72

5.3.2.1 Tone Blocking Signal 72

5.3.2.2 M-PAM Blocking Signal 74

5.3.2.3 M-QAM Blocking Signal 76

5.4 The Effect of the Phase Offset on Performance 78

5.5 The Effectiveness of Blocking Signal Type on Performance 80

5.6 Summary 81

6 Conclusions **83**

Bibliography **87**

List of Figures

1.1 A typical superheterodyne receiver showing the filters, low noise amplifier (LNA), mixer with the local oscillator (LO), intermediate frequency (IF) filter and amplifier, and the demodulator [3] 2

2.1 An example of the effect of power compression on the input/output curve of a receiver with and without nonlinearity. The 1 dB point is the location where the actual output is 1 dB less than the expected output. 11

2.2 The signal amplitude and the third order intermodulation product amplitudes as the input amplitude increases. The location where the two intersect is the IP_3 point. 14

2.3 The effect of nearby interferers on the signal of interest at frequency $2f_1$-f_0 . 15

3.1 A 16-QAM constellation without (a) and with (b) receiver nonlinearity . . . 20

3.2 An 8-PAM constellation without (a) and with (b) receiver nonlinearity . . . 20

3.3 The output of an amplifier when a third order polynomial model is used. α_1 is set to 1 and α_3 is set to -0.1. 22

3.4 The pdf distortion caused by the derivative term for 1D and 2D signals for $\alpha_1 = 1$ and $\alpha_3 = -0.125 + 0.05j$ 24

3.5 The theoretical and simulated pdf of 2-PAM without and with receiver nonlinearity at an SNR of 20 dB 27

3.6 The theoretical and simulated pdf of 4-PAM without and with receiver nonlinearity at an SNR of 20 dB 28

3.7 The theoretical and simulated pdf of 8-PAM without (a) and with (b) receiver nonlinearity at an SNR of 20 dB 28

3.8 The theoretical and simulated pdf of 16-PAM without (a) and with (b) receiver nonlinearity at an SNR of 20 dB 29

3.9 The theoretical and simulated pdf of 8-PAM without (a) and with (b) receiver nonlinearity at an SNR of 15 dB 29

3.10 The theoretical and simulated pdf of 8-PAM without (a) and with (b) receiver nonlinearity at an SNR of 5 dB 30

3.11 The theoretical and simulated pdf of 8-PAM without (a) and with (b) receiver nonlinearity at an SNR of 20 dB 30

3.12 The theoretical and simulated 3D pdf of a 4-QAM signal with $\alpha_1 = 1$ and $\alpha_3 = -0.1 - 0.1j$ viewed from three different angles. 32

3.13 The simulated and theoretical pdfs of 16-QAM without receiver nonlinearity at an SNR of 15 dB 33

3.14 The simulated and theoretical pdfs of 16-QAM with receiver nonlinearity at an SNR of 15 dB, $\alpha_1 = 1$, $\alpha_3 = -0.06$ 33

3.15 The six degrees of receiver nonlinearity that were tested, demonstrated with the signal constellation of an 8-PAM signal at an SNR of 25 dB with and without nonlinearity, $\alpha_1 = 1$ 36

3.16 Three modulated signals with SNR=30 dB, peak power = 1, and $\alpha_1 = 1$, $\alpha_3 = -0.1 - 0.1j$ 37

3.17 The mean squared error of a 2-PAM pdf with six levels of receiver nonlinearity across SNRs from -5 to 20 dB 39

3.18 The mean squared error of an 4-PAM pdf with six levels of receiver nonlinearity across SNRs from -5 to 20 dB 39

3.19 The mean squared error of an 8-PAM pdf with six levels of receiver nonlinearity across SNRs from -5 to 20 dB 40

3.20 The mean squared error of a 16-PAM pdf with six levels of receiver nonlinearity across SNRs from -5 to 20 dB 40

3.21 The mean squared error of a 4-QAM pdf with six levels of receiver nonlinearity across SNRs from -5 to 20 dB 41

4.1 The pdf of a 4-PAM signal with receiver nonlinearity and without (a) and with (b) a tone blocking signal. The SNR=15 dB and $\alpha_1 = 1$ and $\alpha_3 = -0.07$ 46

4.2 The pdf of a 2-PAM signal with 4-PAM interference amplitude levels $[\pm\sqrt{8}, \pm\frac{\sqrt{8}}{3}]$, SNR=15 dB 49

4.3 The mean squared error of a 4-PAM pdf with SNRs from -5 to 20 dB with 5 tone blocker amplitudes. $\alpha_1 = 1$ and $\alpha_3 = -0.07$ 52

4.4 The theoretical and simulated 3D pdf of a 4-QAM signal with tone interference $A_i = 1.5$ with $\alpha_1 = 1$ and $\alpha_3 = -0.07$ for three different viewing angles. . . 53

4.5 The mean squared error of a 4-PAM pdf with a 4-PAM blocker from -5 to 20 dB with 5 blocker peak amplitudes. $\alpha_1 = 1$ and $\alpha_3 = -0.07$ 55

4.6 The theoretical and simulated 3D pdf of a 4-QAM signal with 4-PAM interference $A_i = 5.5$ with $\alpha_1 = 1$, $\alpha_3 = -0.03$, and SNR=15dB for three different viewing angles. 56

4.7 The theoretical and simulated 3D pdf of a 2-PAM signal with a 4-QAM blocker $A_i = \sqrt{\frac{3}{2}}$ with $\alpha_1 = 1$, $\alpha_3 = -0.03$, and SNR=15 dB 59

5.1 Examples of the decision boundaries used to calculate the error rate, both examples have AWGN added 62

5.2 The rectangular decision region around an M-QAM symbol s 64

5.3 The percent error between the simulated and theoretical pdfs across SNRs from -5 to 25 dB for an 8-PAM constellation with varying amounts of receiver nonlinearity 69

5.4 Theoretical and simulated symbol error rates for 8-PAM with varying amounts of nonlinearity. The simulated error rate is averaged over 25 trials. 70

5.5 The symbol error rate of a 4-QAM signal with no nonlinearity and with a severe amount of receiver nonlinearity. 71

5.6 The signal constellation of a 4-QAM signal with and without receiver nonlinearity at an SNR of 15 dB, $\alpha_1 = 1$ and $\alpha_3 = -0.1$ 72

5.7 Theoretical and simulated symbol error rates for 4-PAM with receiver nonlinearity and tone interference of varying amplitudes. E_{av} is the average energy of the 4-PAM signal. 73

5.8 The percent error of the symbol error rate of a 4-PAM signal with 4-PAM blocking signal of varying amplitude 74

5.9 Theoretical and simulated symbol error rates for 4-PAM with receiver nonlinearity and 4-PAM interference of varying average energy. 75

5.10 The percent error of the symbol error rate of a 4-PAM signal with a tone blocking signal of varying amplitude 76

5.11 The simulated signal constellation of a simulated 2-PAM signal with a 4-QAM blocker, $\alpha_1 = 1$, $\alpha_3 = -0.05$, and $A_i = \sqrt{3}$ 77

5.12 The symbol error rate for a simulated 2-PAM signal with 4-QAM interference, $\alpha_1 = 1$, $\alpha_3 = -0.05$, and $A_i = \sqrt{3}$ 77

5.13 The simulated symbol error rate for a 4-PAM signal with 4-PAM interference with two ϕ values. 79

5.14 The received signal constellation of a 4-PAM signal with a 4-PAM blocker with two phase offset values 79

5.15 The simulated symbol error rates of the different blocking signals on 2-PAM, 4-PAM, 8-PAM, and 4-QAM signals of interest. 81

List of Tables

3.1 The six degrees of receiver nonlinearity used to calculate the mean squared error 35

Chapter 1

Introduction and Motivation

Nonlinearity is a critical factor in a receiver that can strongly impact performance. All receiver front ends have some degree of nonlinearity caused by their components that can lead to amplitude and phase distortion in a received signal [1]. Figure 1.1 shows a block diagram of a superheterodyne receiver, a common RF receiver. The portion of the receiver up to the demodulator is considered the front end, and the band pass filter, low noise amplifier, and mixer all contribute to the nonlinearity of the receiver. The four main types of distortion caused by this nonlinearity are power compression, harmonic distortion, cross modulation, and intermodulation distortion. Power compression causes the amplitude and phase distortion seen in the received symbols of a signal and occurs when the power of the received signal causes the receiver to operate in its saturation region. While frequency modulated signals tend to be fairly immune to power compression effects even small amounts of nonlinearity cause compression in amplitude modulated signals. Harmonic distortion leads to the generation of signal components at multiples of the transmitting frequency. These

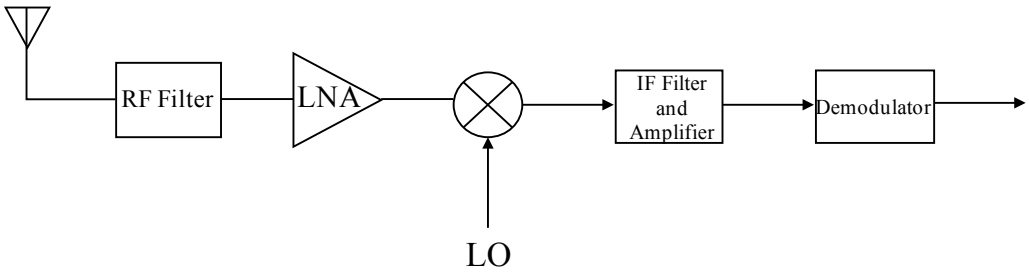

Figure 1.1: A typical superheterodyne receiver showing the filters, low noise amplifier (LNA), mixer with the local oscillator (LO), intermediate frequency (IF) filter and amplifier, and the demodulator [3]

components can often be filtered out at the receiver and tend to not impact performance in most situations. Cross modulation leads to the transfer of an interfering signals' modulation onto the signal of interest, and occurs when an adjacent channel interfering signal is within the passband of the RF filter at the receiver. Finally, intermodulation distortion occurs when the receiver nonlinearity leads to the generation of signal components at nearby frequencies when two or more signals are received and combined nonlinearly. For example, two signals at frequencies f_0 and f_1 will generate frequency components at $2f_0 - f_1$, $2f_1 - f_0$, $3f_0 - 2f_1$, $3f_1 - 2f_0$ and so on. Two signals close to the frequency of a signal of interest, either intentional jamming signals or unintentional interference, can therefore lead to a reduction in performance of the desired signal due to this distortion [2].

Power compression, intermodulation distortion, and cross modulation increase the error rates of amplitude modulated signals, such as M-PAM and M-QAM. However, using simulation to calculate the impact of the receiver nonlinearity is a time consuming process.

Therefore, deriving error rate expressions that take into account the effect of receiver nonlinearity is important for design purposes. Some previous work has focused on deriving error rate expressions for transmitter nonlinearity, which has a similar model to receiver nonlinearity, however transmitter nonlinearity does not lead to distortion of the effects of the channel on the signal. For example, the noise added to a signal from an additive white Gaussian noise (AWGN) channel would also undergo nonlinear distortion. [4] analyzes the effect of a nonlinear power amplifier on the bit error rate of filter bank-based multicarrier using offset QAM (FBMC/OQAM) and orthogonal frequency division multiplexing (OFDM) signals through AWGN and Rayleigh fading channels. Bit error rate expressions for these signals are derived when polynomial fitting is used to model the power amplifier. [5] analyzes the effect of power amplifier nonlinearity on the bit error rate of 16-QAM and 64-QAM signals by simulating the signals and measuring the degradation of the symbol and bit error rates. [6], [7], [8], [9], and [10] analyze the effects of transmitter nonlinearity on the performance of OFDM signals and provide quantitative measurements of the performance decrease. [11] develops a technique for receiver design that can compensate for nonlinearity caused by the power amplifier in the transmitter. Finally, [12] develops analytical expressions for the bit error rates of a QPSK modulated CDMA system in the presence of transmitter nonlinearity. While these works demonstrate that the amplitude and phase distortions caused by transmitter nonlinearity lead to a decrease in performance, they are not entirely applicable to receiver nonlinearity due to the additional distortion caused by the channel effects.

Previous work has also analyzed the impact of receiver nonlinearity on performance. [13]

describes the importance of determining the impact of receiver nonlinearity on performance as spectrum becomes more crowded and interference generated by adjacent channel signals becomes a larger problem. Due to the higher amount of RF interference with the rise of spectrum sharing, "receivers will likely operate in the nonlinear region of the RF front-end in next generation networks" [13]. Additionally, theoretical expressions are derived for the achievable rates when receiver nonlinearity is present and when adjacent channel interference is present. [14] discusses spectrum sharing when receiver nonlinearity is present and develops an algorithm for channel assignment to minimize the impact of adjacent channel interference caused by the nonlinearity. [15] derives expressions for AWGN and Rayleigh fading channel capacity to optimize receiver design. [16] analyzes the impact of amplitude modulated blocking signals on the performance of PSK signals of interest. Finally, [17] derives theoretical symbol error rates for M-PSK signals with M-PSK blocking signals and receiver nonlinearity. The impact of amplitude modulated blocking signals on amplitude modulated signals of interest is a topic that has not been previously examined.

While receiver nonlinearity negatively impacts performance, there are several techniques to mitigate this impact. [18] discusses a method to compensate for cross modulation generated by a blocking signal by processing the blocking signal and the desired signal separately at the receiver, estimating the nonlinearity, and then recovering the original data symbols. [19], [20], [21], and [22] discuss equalization methods for cancelling the effects of third-order intermodulation products at the receiver. [23] and [24] discuss two linearization methods to mitigate the nonlinear distortions caused by the components in the receiver. Finally,

[25] describes the optimal operating location for a cognitive radio receiver based on the intermodulation distortion present. While mitigating the harmful interference caused by nonlinearity can improve the error rate of a wireless system, this is not always the most "optimum spectrum policy" [26] and in some cases the receiver will need to operate in its nonlinear region.

Because wireless receivers will not always operate in their linear region, it is necessary to quantify how the nonlinearity will negatively impact the performance. [27] discusses a method to derive the probability density function of a BPSK signal with receiver nonlinearity by using a change of variables technique, which incorporates the effect of the nonlinear distortion on the AWGN added from the channel. This thesis uses this change of variables method to model the probability density function and derive theoretical error rates for M-PAM and M-QAM signals with receiver nonlinearity with and without desensitization effects caused by the presence of adjacent channel interference. In contrast to other works, expressions will be derived to analyze the impact of nonlinearity on the distribution of the received symbols. These pdfs will be used to derive theoretical bit and symbol error rate expressions for any M-PAM and rectangular M-QAM signal. Finally, simulations in Matlab will be used to show the accuracy of the pdf and BER expressions. The derived expressions reported in this thesis will provide a relationship between performance and the amount of receiver nonlinearity. For a certain performance requirement, the maximum allowable amount of distortion can be calculated and then a wireless receiver can be chosen to meet this linearity requirement.

1.1 Thesis Outline and Research Contributions

There are three main research contributions described in this thesis:

- The derivation of probability density functions for M-PAM and M-QAM signals in the presence of receiver nonlinearity
- The derivation of theoretical bit and symbol error rates for these signals with receiver nonlinearity
- The derivation of probability density functions and error rates for these signals in the presence of adjacent channel interference.

This thesis is organized into six chapters:

- Chapter 2 provides a background on the distortion effects caused by receiver nonlinearity and the memoryless polynomial model for representing receiver nonlinearity
- Chapter 3 discusses how pdfs can be derived for signals with receiver nonlinearity and derives expressions for M-PAM and M-QAM signals
- Chapter 4 extends Chapter 3 and derives pdf expressions for M-PAM and M-QAM signals in the presence of tone, M-PAM, and M-QAM adjacent channel interference
- Chapter 5 derives theoretical bit and symbol error rates from the pdfs derived in Chapters 3 and 4 and provides performance plots for various nonlinearity scenarios
- Chapter 6 summarizes the results and discusses future work

Chapter 2

Receiver Nonlinearity

This chapter describes the characteristics of an RF front end and how the various components can lead to nonlinear distortion. It will also describe how the nonlinearity can be modeled with a memoryless polynomial model as well as the four major distortion effects caused by receiver nonlinearity. These effects will degrade the performance of amplitude modulated signals by distorting the received signal constellation and by generating intermodulation products at the frequency of interest.

2.1 Characteristics of an RF Front End

Figure 1.1 shows a block diagram of a typical wireless receiver. Most RF front ends have a band pass filter, which removes unwanted signal components, a low noise amplifier (LNA) to amplify the received signal, a mixer, and an analog to digital converter (ADC). Each component has some degree of nonlinearity that contributes to the overall nonlinearity of

the receiver. [28] shows an example of the contribution of the front end components to the total receiver nonlinearity for a dual Bluetooth/WiFi receiver. The LNA and filter contribute about 30% each to the nonlinearity, while the mixer contributes around 40%.

2.2 RF Front End Modeling - Polynomial Model

A nonlinear receiver front-end will introduce amplitude and phase distortions in a received signal. For simulation and analysis purposes, it is necessary to have accurate receiver front-end models that are not computationally complex.

The most simple model of a nonlinear RF front end is the memoryless polynomial model. This model is a narrowband approximation of a receiver that does not take into account memory effects that depend on the frequency or bandwidth of the signal [29]. The bandpass version of this model is a power series, modeled as [30]:

$$y(t) = \sum_{k=1}^{L} \alpha_k x^k(t) \tag{2.1}$$

where $x(t)$ is the received signal, $y(t)$ is the received signal taking into account the nonlinear distortion, L is the order of the polynomial, and $\alpha_k, k = 1, 2, ..$ are coefficients representing the amount of nonlinearity in the system. The coefficient α_1 is the linear gain caused by the front end. When only amplitude distortions are present, these coefficients are real. However, often both amplitude and phase distortions are present, requiring the use of complex coefficients. The baseband version of the polynomial model is similar, but requires a slight

modification [31]. This equation, which will be the model used throughout this thesis is:

$$y(t) = \sum_{k=1}^{L} \alpha_k x(t)|x(t)|^{k-1} \tag{2.2}$$

The even order terms produce distortion products far from the frequency of interest that can be filtered out at the output, but the odd order terms produce products close to the signal of interest that can cause significant distortion. Out of these odd order terms, the third order term produces products that are generally the highest in power and closest to the frequency of interest. Therefore, this equation can be simplified to

$$y(t) = \alpha_1 x(t) + \alpha_3 x(t)|x(t)|^2 \tag{2.3}$$

and would be an acceptably accurate model of the nonlinearity. The complex coefficients can be determined by polynomial fitting with measurements found from the front-end, such as spurious-free dynamic range measurements [32]. While memory effects are present in wireless receivers and cannot be ignored for wideband signals, this third degree memoryless polynomial model is widely used as an approximation for performance analysis as shown in [2], [4], [13], [14], [17], [27], [33], [34], and [35]. The derived expressions for the pdfs and error rates of received signals with nonlinearity use the approximation in (2.3), but the derivation process will be the same for any function that relates the nonlinearly received signal to the same signal without nonlinearity.

2.3 Effects of a Nonlinear Receiver

There are four main types of nonlinear effects: power compression, harmonic distortion, intermodulation distortion, and cross modulation [15]. These effects are described in this section, using the polynomial model for demonstration.

2.3.1 Power Compression

Power compression is a nonlinear effect that occurs in all receivers because the supply voltage will limit the output power. As the input power into a receiver increases, the output power also increases, up to a point where compression occurs. A common measure of compression is the 1-dB compression point, which is the location at which the output power has decreased by 1 dB from its expected linear value. Figure 2.1 shows this compression point. Suppose the received signal is the sinusoid $A\cos(2\pi ft)$. Using a third degree polynomial model, the received signal $y(t)$ with nonlinearity will be

$$y(t) = \alpha_1 A\cos(2\pi ft) + \alpha_3\left(\frac{3}{4}A^3\cos(2\pi ft) + \frac{1}{4}A^3\cos(3(2\pi ft))\right)$$

Therefore at the frequency of interest f, the amplitude of the received sinusoid will be $(\alpha_1 A + \frac{3}{4}\alpha_3 A^3)$ and the gain will be $\alpha_1 + \frac{3}{4}\alpha_3 A^2$. Usually, α_1 is positive and α_3 is negative, so the α_3 term will cause the output amplitude to decrease as the input amplitude increases, leading to amplitude compression. While frequency and phase modulated signals are resistant to compression effects, amplitude modulated signals can be strongly affected [2]. Therefore the effects of nonlinearity on QAM and PAM modulated signals are considered.

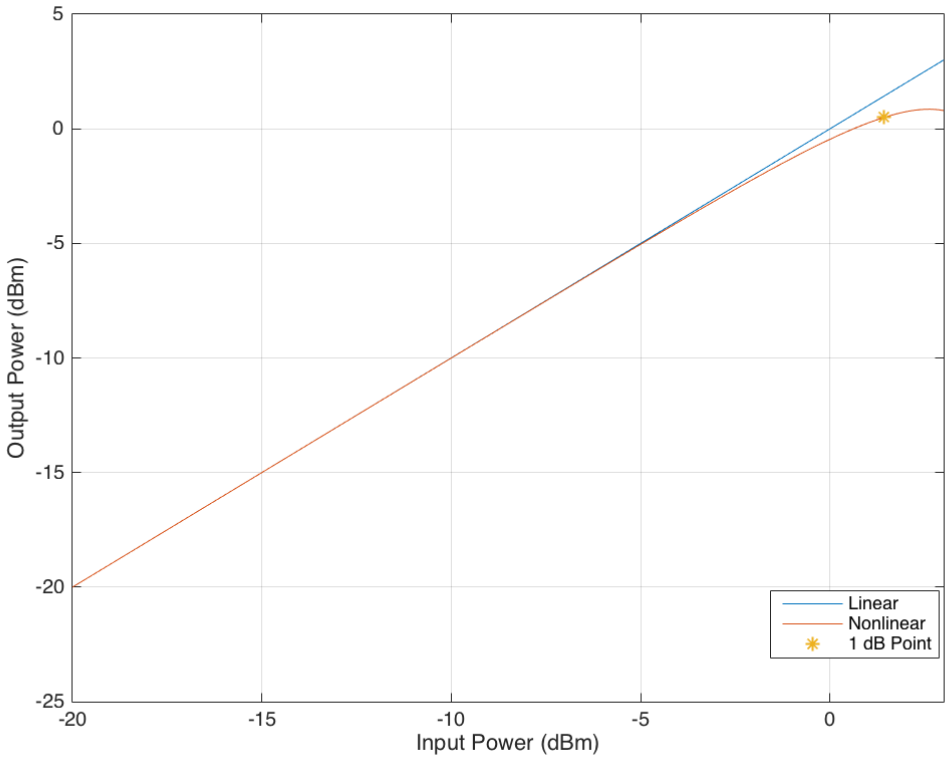

Figure 2.1: An example of the effect of power compression on the input/output curve of a receiver with and without nonlinearity. The 1 dB point is the location where the actual output is 1 dB less than the expected output.

2.3.2 Harmonic Distortion

Harmonic distortion leads to the generation of signals at frequency multiples of the desired frequency. Using the polynomial model $y(t) = \alpha_1 x(t) + \alpha_2 x(t)^2 + \alpha_3 x(t)^3$ to show all the generated harmonic components, and a transmitted signal $x(t) = A\cos(2\pi ft)$, $y(t)$ will become:

$$y(t) = \alpha_1 A\cos(2\pi ft) + \alpha_2 A^2\cos^2(2\pi ft) + \alpha_3 A^3\cos^3(2\pi ft)$$

$$y(t) = \frac{\alpha_2}{2}A^2 + (\alpha_1 A + \frac{3\alpha_3}{4}A^3)\cos(2\pi ft) + \frac{\alpha_2}{2}A^2\cos(4\pi ft) + \frac{\alpha_3}{4}A^3\cos(6\pi ft)$$

This demonstrates the generation of frequency components at 2x and 3x the original frequency, as well as a DC offset due to the receiver nonlinearity. However, the harmonic components normally do not affect the received signal significantly because they can be filtered out in most cases [2].

2.3.3 Intermodulation

Intermodulation products are frequency components that are generated as a result of two or more signals being transmitted at close frequencies. For example, suppose the input signal is $x(t) = A_1\cos(2\pi f_1 t) + A_2\cos(2\pi f_2 t)$. With nonlinearity and using the third order memoryless polynomial model in (2.3), intermodulation products will be generated at the equally spaced frequencies $2f_1 - f_2$, f_1, f_2, and $2f_2 - f_1$ within the band of interest. The amplitudes of these products will be [35]:

$$2f_1 - f_2\text{: } \tfrac{3\alpha_3 A_1^2 A_2}{4}$$

$$f_1\text{: } \alpha_1 A_1 + \tfrac{3}{4}\alpha_3 A_1^3 + \tfrac{3}{2}\alpha_3 A_1 A_2^2$$

$$f_2\text{: } \alpha_1 A_2 + \tfrac{3}{4}\alpha_3 A_2^3 + \tfrac{3}{2}\alpha_3 A_2 A_1^2$$

$$2f_2 - f_1\text{: } \tfrac{3\alpha_3 A_1 A_2^2}{4}$$

For a higher order polynomial model, intermodulation products will be generated at frequencies $|\pm pf_1 \pm qf_2|$, where p and q are positive integers [13]. The third order terms $2f_1 - f_2$

and $2f_2 - f_1$ will be closer to the frequency of interest than the fifth order terms $3f_1 - 2f_2$ and $3f_2 - 2f_1$, which will be closer than the seventh order terms, and so on. Because the third order terms are the largest contributor to the distortion, the simplified third order polynomial model can be used [13].

The third-order intercept point IP_3 is a common measure of the distortion caused by two received tones. Figure 2.2 shows a graph of the amplitude of the tone input compared with the amplitude of the third order products. The location where the two lines intersect, where the amplitude of the third order intermodulation products is the same as the amplitude of the two signals, is the IP_3 point [36]. The input level where the point occurs is known as the IIP_3 point and the output level is the OIP_3 point. While this is a theoretical point because the receiver will saturate before this point occurs, it is a good measure of the amount of nonlinearity in the receiver and can be compared between devices. Receivers with a high IP_3 are more linear than receivers with a low IP_3. For a third order polynomial model, the IIP_3 of the receiver in terms of α_1 and α_3 is

$$IIP_3 = \sqrt{\frac{4}{3}\left|\frac{\alpha_1}{\alpha_3}\right|} \tag{2.4}$$

The IIP_3 is measured in dBm, and represents the total amount of nonlinearity caused by the components in the RF front-end [2]. Wi-Fi receivers tend to be fairly nonlinear, for example the Wi-Fi receiver in reference [28] has an IIP_3 of -13 dBm. Receivers for 3G and LTE tend to be more linear. The LTE receiver in [37] has an IIP_3 value of 0 dBm. A common interference or jamming scenario occurs when two blocking signals are present at frequencies f_1 and f_2 while the signal of interest is being transmitted at frequency $2f_2 - f_1$.

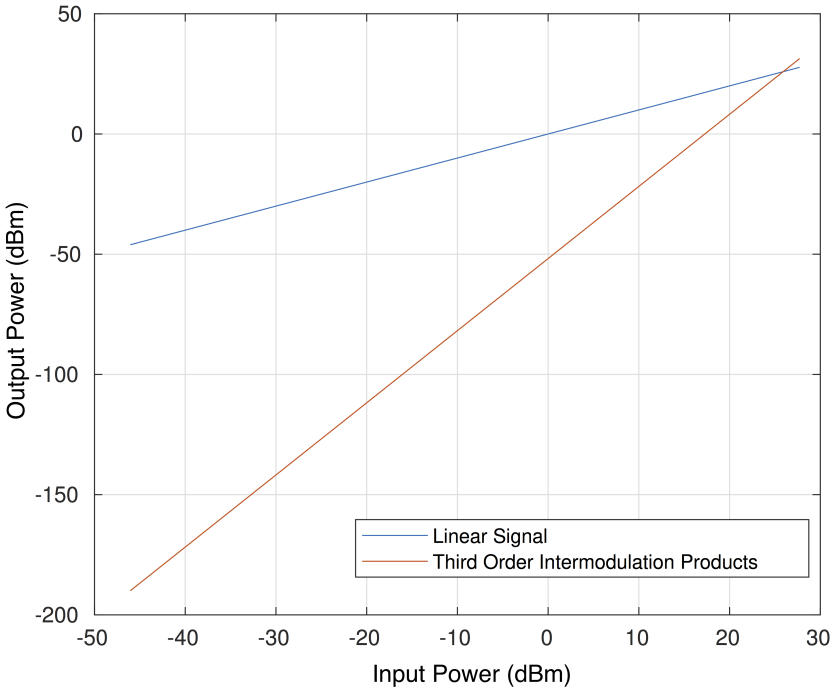

Figure 2.2: The signal amplitude and the third order intermodulation product amplitudes as the input amplitude increases. The location where the two intersect is the IP_3 point.

Figure 2.3 shows a diagram of this situation. The interferers will create an intermodulation product at $2f_1 - f_1$ that will decrease the error rate of the signal of interest. If the power of the interfering signals is significant enough, the amplitude of the intermodulation product will be large enough to completely block all communication at $2f_2 - f_1$. In contrast to co-channel interference, this adjacent channel interference cannot be mitigated by increasing the transmitted power of the signal of interest [13].

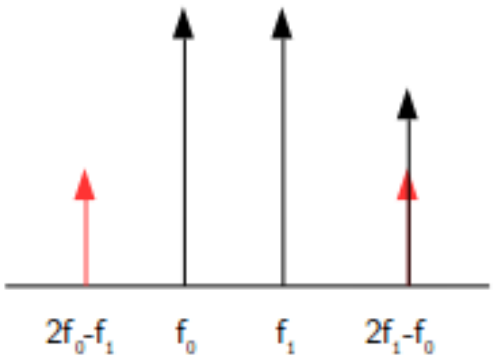

Figure 2.3: The effect of nearby interferers on the signal of interest at frequency $2f_1$-f_0

2.3.4 Cross Modulation

Cross modulation occurs when a modulated interfering signal transfers its modulation characteristics to a neighboring signal when both signals enter a nonlinear receiver. The most common example is a high powered amplitude modulated signal close to a signal of interest. For example, if an interferer is at frequency f_0 in Figure 2.3 and the desired signal is at frequency f_1, then the received amplitude at f_1 would be $\alpha_1 A_2 + \frac{3}{4}\alpha_3 A_2^3 + \frac{3}{2}\alpha_3 A_2 A_1^2$ due to the nonlinearity, where A_1 is the amplitude of the interfering signal [38]. For an amplitude modulated interferer, this would cause the amplitude modulation of the interfering signal to be transferred to the desired signal. For memoryless nonlinear systems, amplitude modulation is usually the cause of cross modulation, but phase modulation can cause cross modulation when the nonlinear system has memory [2].

2.4 Summary

Receiver nonlinearity can compress and rotate the received symbols in an amplitude modulated signal, leading to a decrease in performance. This nonlinearity is caused by all of the components in a receiver front end and there is always some degree of nonlinearity present. Additionally, high powered signals that are located at frequencies nearby to a signal of interest can generate intermodulation products and desensitize the signal of interest. Chapters 3, 4, and 5 derive theoretical probability density functions and error rate expressions for M-PAM and M-QAM signals with and without interference caused by a nearby blocking signal.

Chapter 3

Modeling the Probability Density Functions of Amplitude Modulated Signals with Receiver Nonlinearity

This chapter describes the impact of the nonlinear distortion caused by the receiver on the received constellation in an AWGN channel, as well as describes a technique in which the probability density function (pdf) of the signal can be derived by using a change of variables to write the nonlinear pdf in terms of the perfectly linear pdf. Matlab simulation demonstrates that these pdf expressions are just as accurate for measuring the distribution of a nonlinear signal as the accepted expressions when no nonlinearity is present.

3.1 M-PAM and M-QAM Modulation

M-PAM and M-QAM are two amplitude modulation schemes for wireless signals. For M-PAM, each pulse has a varying amplitude that can be one of $2m - 1 - \mathrm{M}$, where M is the modulation order of the signal. For a modulated bandpass signal, PAM can be represented as:

$$s(t) = A_m g(t) \cos(2\pi f t) \tag{3.1}$$

where A_m is the set of pulse amplitudes, $g(t)$ is the transmitting pulse (commonly a root-raised cosine pulse), and f is the frequency of interest [39]. This results in a one-dimensional signal constellation with equidistant symbols.

M-QAM is a two dimensional extension of M-PAM that modulates the information symbols onto two carrier signals. Similar to M-PAM, the signal can be expressed as:

$$s(t) = A_{mi} g(t) \cos(2\pi f t) - j A_{mq} g(t) \sin(2\pi f t) \tag{3.2}$$

where A_{mi} and A_{mq} are the in-phase and quadrature amplitudes respectively [39]. This results in a signal constellation that is both amplitude modulated and phase modulated. QAM allows for high data rates and is thus used for LTE and 802.11ac. These applications use rectangular M-QAM constellations, so rectangular QAM will be assumed when deriving the theoretical probability density functions. However, these techniques can be expanded to derive expressions for irregular QAM constellations.

3.2 Signal Constellation Distortion Due to Receiver Nonlinearity

Receiver nonlinearity leads to AM-AM and AM-PM conversions, which are visible in the received signal constellation as a compression and rotation of the symbols. Symbols with higher power are affected stronger by nonlinear distortion, thus the outer points in a signal constellation tend to be visibly distorted while the inner points tend to be less affected. When a memoryless polynomial model is used, each complex α_k adds amplitude and phase distortion. Figure 3.1 demonstrates the effect of receiver nonlinearity on a rectangular 16-QAM signal constellation. Figure 3.2 shows a stronger amount of receiver nonlinearity on an 8-PAM constellation. The outer points in the constellation have become much more compressed towards the center of the constellation and rotated. The amplitude and phase distortion caused by receiver nonlinearity leads to distortions in the probability density functions of the signals.

3.3 Determining Probability Density Function Expressions for Receivers with Nonlinearity in an AWGN Channel

When a memoryless polynomial model is used to model the receiver nonlinearity and the signal passes through an AWGN channel, the received signal y can be written in terms of

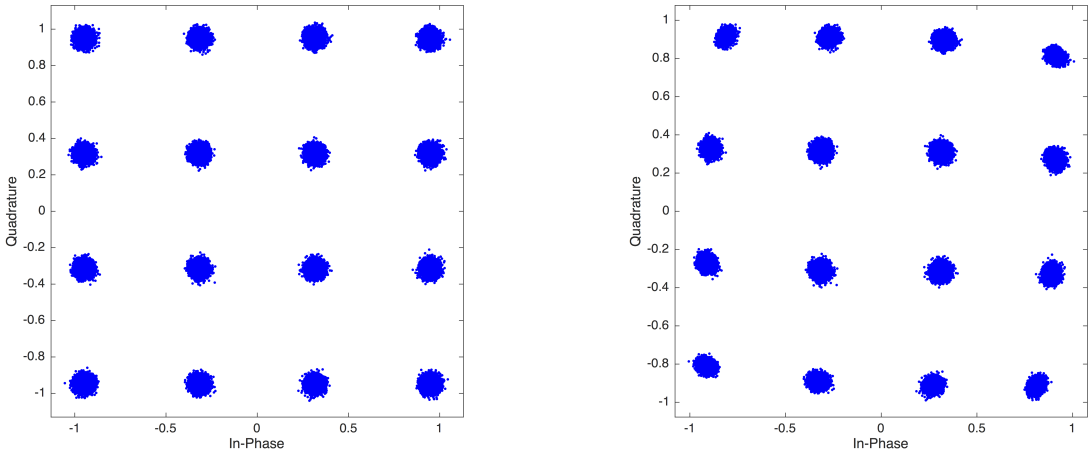

(a) Perfectly linear receiver

(b) $\alpha_1 = 1$, $\alpha_3 = -0.05 - 0.03j$

Figure 3.1: A 16-QAM constellation without (a) and with (b) receiver nonlinearity

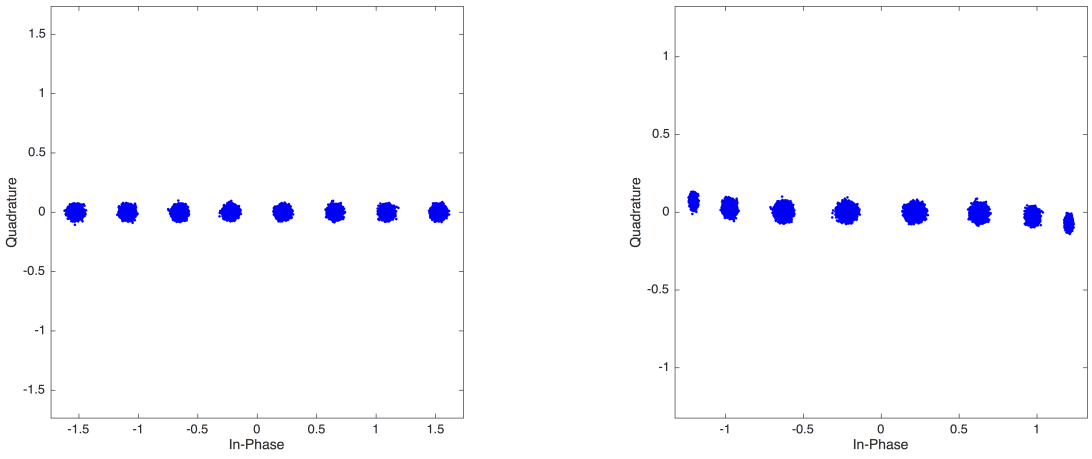

(a) Perfectly linear receiver

(b) $\alpha_1 = 1$, $\alpha_3 = -0.09 - 0.02j$

Figure 3.2: An 8-PAM constellation without (a) and with (b) receiver nonlinearity

the transmitted signal x and additive white Gaussian noise n as

$$y = \sum_{k=1}^{K} \alpha_k (x+n)|(x+n)|^{k-1} \tag{3.3}$$

where K is the highest order polynomial in the model. Because the even order components can be removed with filtering, this model can be simplified to

$$y = \sum_{k=1}^{\frac{K+1}{2}} \alpha_{2k-1} (x+n)|(x+n)|^{2k-2} \tag{3.4}$$

If the probability of symbol error was calculated directly from this equation, the resulting expression would have squared, cubic, and higher order noise terms thus making the calculation extremely complex. To mitigate this complexity, a change of variables can be used to write the nonlinearly received signal in terms of the pdf of a perfectly linear receiver.

3.3.1 Using a Change of Variables to Derive the PDF for a Nonlinear Receiver

Suppose (3.4) is used to model the effects of receiver nonlinearity. Figure 3.3 shows a plot of this function with the values $\alpha_1 = 1$ and $\alpha_3 = -0.1$ with the remaining α_k set to 0. The inverse of this function will have 1 solution for each value of y. The pdf of $y = g(x)$ can be written in terms of the pdf of x using a change of variables, where N is the number of solutions for $y = g(x)$, as [40]

$$f_y(y) = \sum_{n=1}^{N} f_x(g_n^{-1}(y)) \left| \frac{\partial}{\partial y} g_n^{-1}(y) \right| \tag{3.5}$$

or

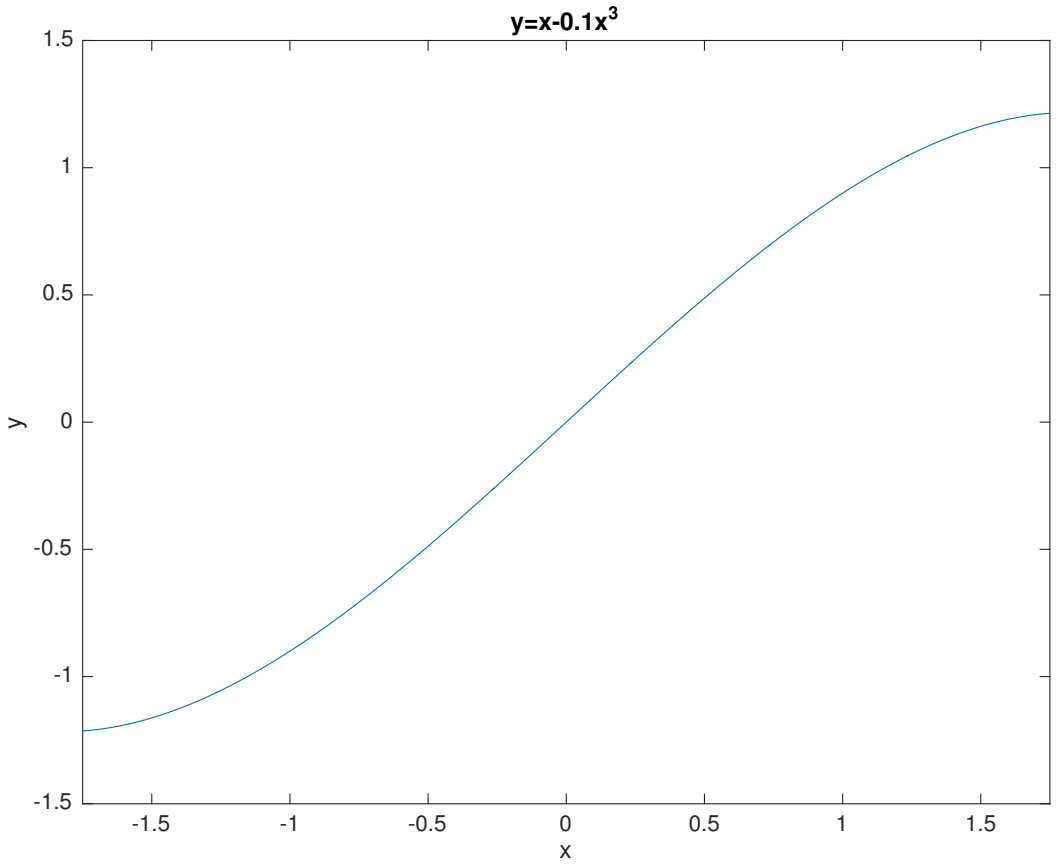

Figure 3.3: The output of an amplifier when a third order polynomial model is used. α_1 is set to 1 and α_3 is set to -0.1.

$$f_y(y) = \frac{f_x(g_1^{-1}(y))}{|g'(x_1)|} + \frac{f_x(g_2^{-1}(y))}{|g'(x_2)|} + ... + \frac{f_x(g_N^{-1}(y))}{|g'(x_N)|} \tag{3.6}$$

where x_i's are the solutions for $g^{-1}(y)$ for each y. When $y = g(x)$ is monotonic, which will usually be the case for a receiver model, N will equal 1 [27]. Therefore, the remainder of this thesis will assume the polynomial model is monotonic. When $y = g(x)$ is a third order

memoryless polynomial (3.6) can be simplified to [27]

$$f_y(y) = \frac{f_x(g^{-1}(y))}{|\alpha_1 + 3\alpha_3(g^{-1}(y))^2|} \tag{3.7}$$

When a higher order polynomial model is used, the general form of this equation would be

$$f_y(y) = \frac{f_x(g^{-1}(y))}{\sum_{k=1}^{L} |(2k-1)\alpha_{2k-1}(g^{-1}(y))^{2k-2}|} \tag{3.8}$$

where $2L-1$ is the highest order polynomial in the model. The $\frac{1}{\sum_{k=1}^{L}\left|(2k-1)\alpha_{2k-1}(g^{-1}(y))^{2k-2}\right|}$ portion of this expression largely contributes to the distortion of the pdf seen for amplitude modulated signals. Figure 3.4 shows this expression for a 1D signal such as PAM and a 2D signal such as QAM. Outer symbols will be affected more strongly than inner symbols, and the pdf will be distorted following the functions represented in these figures. While the model for the pdf with receiver nonlinearity is applicable to any order polynomial model, this thesis focuses on third order models. Once the pdf is derived for a modulated signal, it can be used to find the theoretical bit and symbol error rates.

3.3.2 Probability Density Functions of M-PAM and M-QAM Signals with a Nonlinear Receiver

3.3.2.1 Modeling the PDF of M-PAM Signals with a Nonlinear Receiver

A received M-PAM signal will have M symbols at positions $(2i - \mathrm{M} - 1)\sqrt{E_b/E_{av}}$ on the real axis, where $i = 0, ..., \mathrm{M}-1$ and E_b is the energy per bit and E_{av} is the average energy for the constellation. To calculate the probability density function for any M-PAM constellation, it will be assumed that the channel is AWGN and there is an equal probability of each symbol.

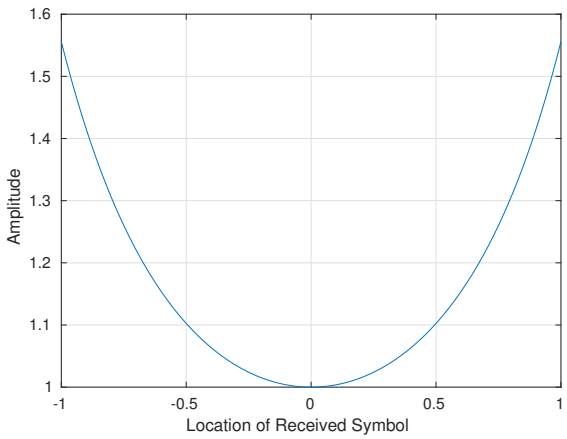

(a) PAM

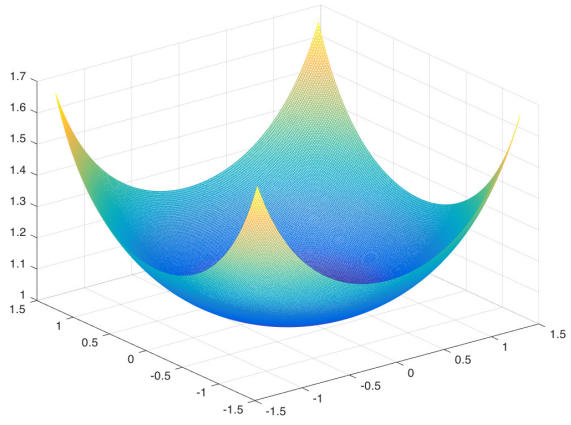

(b) QAM

Figure 3.4: The pdf distortion caused by the derivative term for 1D and 2D signals for $\alpha_1 = 1$ and $\alpha_3 = -0.125 + 0.05j$

The received signal y assuming perfect linearity can be represented by $y = x_k + n$, $k = 1, ...\mathrm{M}$, where x_k is a symbol in the M-PAM modulated signal and n is AWGN. The pdf of the noise component follows the Gaussian distribution:

$$f(n) = \frac{1}{\sqrt{2\pi\sigma^2}} e^{\frac{-n^2}{2\sigma^2}} \tag{3.9}$$

where $\sigma = \frac{N_0}{2}$. Therefore, $f(y) = \frac{1}{\mathrm{M}} \sum_{k=1}^{\mathrm{M}} f(y|x_k)$. Each $f(y|x_k)$ can be modeled with the following distribution:

$$f(y|x_k) = \frac{1}{\sqrt{2\pi\sigma^2}} e^{\frac{-(y-x_k)^2}{2\sigma^2}} \tag{3.10}$$

Therefore, the total probability density function will be

$$f(y) = \frac{1}{\mathrm{M}} \sum_{k=1}^{\mathrm{M}} \frac{1}{\sqrt{2\pi\sigma^2}} e^{\frac{-(y-x_k)^2}{2\sigma^2}} \tag{3.11}$$

When the receiver is nonlinear, the pdf can be modeled according to (3.8) by substituting the result from (3.11) as $f_x(\mathrm{x})$. This results in the following pdf for the nonlinear output y for any odd-order memoryless polynomial model:

$$f_y(y) = \frac{1}{\mathrm{M}\sum_{k=1}^{L}|(2k-1)\alpha_{2k-1}(g^{-1}(y))^{2k-2}|}\sum_{m=1}^{\mathrm{M}}\frac{1}{\sqrt{2\pi\sigma^2}}e^{\frac{-(g^{-1}(y)-x_m)^2}{2\sigma^2}} \tag{3.12}$$

The 2D pdf is commonly used to find theoretical bit and symbol error rates for an M-PAM signal. However for severe amounts of phase distortion in the constellation due to nonlinearity, this equation will not hold due to the distortion along the imaginary axis, and the 3D linear pdf of the M-PAM signal should be used for $f_x(\mathrm{x})$.

3.3.2.2 Modeling the PDF of M-QAM Signals with a Nonlinear Receiver

The probability density function of M-QAM is derived in a similar way to M-PAM. The symbol points for a rectangular M-QAM constellation are received at the locations $A_{mi}+jA_{mq}$ where A_{mi} and A_{mq} are one of $(2i-\mathrm{M}-1)\sqrt{E_b/E_{av}}$. Assuming an AWGN channel, equal probability of each symbol, and equal variances for both the I and Q components, the probability density function $f(x,y) = \frac{1}{\mathrm{M}}\sum_{k=1}^{\sqrt{\mathrm{M}}}\sum_{l=1}^{\sqrt{\mathrm{M}}} f((x,y)|(x_k,y_l))$ is modeled as follows:

$$f((x,y)|(x_k,y_l)) = \frac{1}{\sqrt{2\pi\sigma^2}}e^{\frac{-(x-x_k)^2}{2\sigma^2}} * \frac{1}{\sqrt{2\pi\sigma^2}}e^{\frac{-(y-y_l)^2}{2\sigma^2}} = \frac{1}{2\pi\sigma^2}e^{\frac{-((x-x_k)^2+(y-y_l))^2}{2\sigma^2}} \tag{3.13}$$

This pdf is the product of two independent $\sqrt{\mathrm{M}}$-PAM pdfs. The total probability density function $f(x,y)$ would therefore be:

$$f(x,y) = \frac{1}{\mathrm{M}}\sum_{k=1}^{\sqrt{\mathrm{M}}}\sum_{l=1}^{\sqrt{\mathrm{M}}}\frac{1}{2\pi\sigma^2}e^{\frac{-((x-x_k)^2+(y-y_l))^2}{2\sigma^2}} \tag{3.14}$$

For a nonlinear receiver, this pdf will be modified according to equation 3.8 to account for the amplitude and phase distortions. For one symbol, where x' and y' are the transformed x and y:

$$f_{x',y'}(x',y') = \frac{\left|\frac{\partial}{\partial y}g^{-1}(x')\right|}{\sqrt{2\pi\sigma^2}} e^{\frac{-(g^{-1}(x')-x_k)^2}{2\sigma^2}} * \frac{\left|\frac{\partial}{\partial y}g^{-1}(y')\right|}{\sqrt{2\pi\sigma^2}} e^{\frac{-(g^{-1}(y')-y_l)^2}{2\sigma^2}} \tag{3.15}$$

This leads to the final pdf for a rectangular M-QAM signal with receiver nonlinearity:

$$f_{x',y'}(x',y') = \frac{1}{\mathrm{M}} \frac{\sum_{k=1}^{\sqrt{\mathrm{M}}}\sum_{l=1}^{\sqrt{\mathrm{M}}} \frac{1}{2\pi\sigma^2} e^{\frac{-((g^{-1}(x')-x_k)^2+(g^{-1}(y')-y_l))^2}{2\sigma^2}}}{\sum_{k=1}^{L}|(2k-1)\alpha_{2k-1}(g^{-1}(x'))^{2k-2}| * \sum_{k=1}^{L}|(2k-1)\alpha_{2k-1}(g^{-1}(y'))^{2k-2}|} \tag{3.16}$$

3.4 Comparison of Theoretical PDF Expressions with Simulated PDF Expressions

3.4.1 Simulated and Theoretical Probability Density Functions

To determine the validity of the derived probability density function expressions for M-PAM and rectangular M-QAM with a nonlinear receiver, Matlab was used to simulate the modulated signals through an AWGN channel with varying receiver nonlinearity values. A vector of random symbols with equal probability was generated and then the symbols were modulated, AWGN was added, a memoryless polynomial model added nonlinearity, and finally the symbols were demodulated. Rectangular pulse shaping was assumed. A histogram of the nonlinearly received signal was created using the built-in Matlab function "histogram" with "Normalization" set to "pdf" and a bin size of 0.01 to create the simulated pdf of each signal with the theoretical pdf overlaid to compare the accuracy.

To determine the validity of the M-PAM pdf expressions, the pdf was modeled for 2-PAM, 4-PAM, 8-PAM, and 16-PAM with the theoretical expressions overlaid. This section shows qualitative results, while Section 3.4.2 provides quantitative measurements of the accuracy of the expressions. These qualitative results are shown in Figures 3.5, 3.6, 3.7, and 3.8 for a peak power of 1, SNR of 20 dB, and a moderate amount of receiver nonlinearity, with the simulated pdf averaged over 25 iterations. These figures show that the theoretical pdf expressions overlap the simulated pdf expressions very accurately. Additionally, Figure 3.9 shows the simulated and theoretical pdfs of 8-PAM at an SNR of 15 dB, Figure 3.10 shows the pdfs of 8-PAM at an SNR of 5 dB, and Figure 3.11 shows the pdfs of 8-PAM with a higher amount of receiver nonlinearity. Even at lower SNRs and higher amounts of nonlinearity, the simulated and theoretical results still overlap accurately.

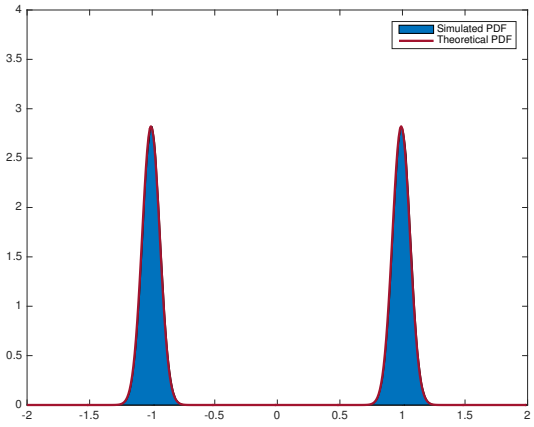

(a) Perfectly linear receiver

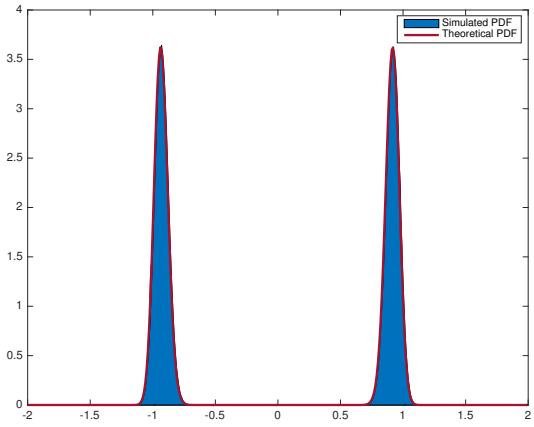

(b) $\alpha_1 = 1$, $\alpha_3 = -0.075 - 0.025j$

Figure 3.5: The theoretical and simulated pdf of 2-PAM without (a) and with (b) receiver nonlinearity at an SNR of 20 dB

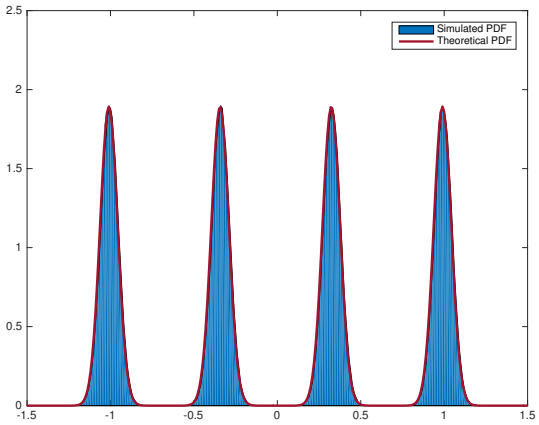

(a) Perfectly linear receiver

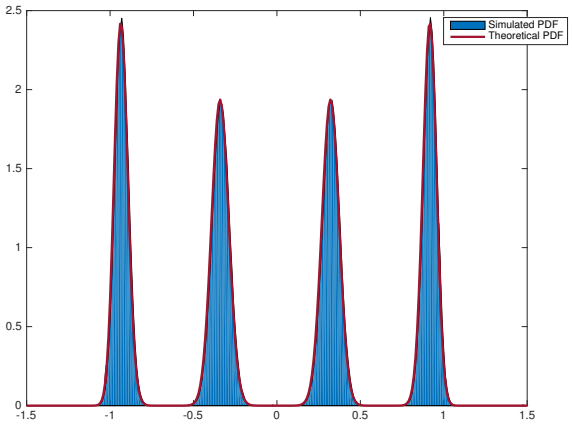

(b) $\alpha_1 = 1$, $\alpha_3 = -0.075 - 0.025j$

Figure 3.6: The theoretical and simulated pdf of 4-PAM without (a) and with (b) receiver nonlinearity at an SNR of 20 dB

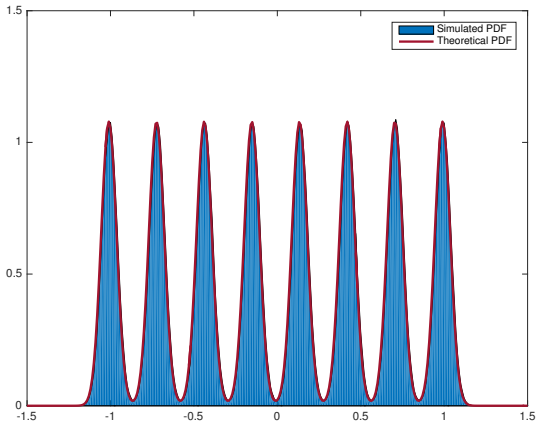

(a) Perfectly linear receiver

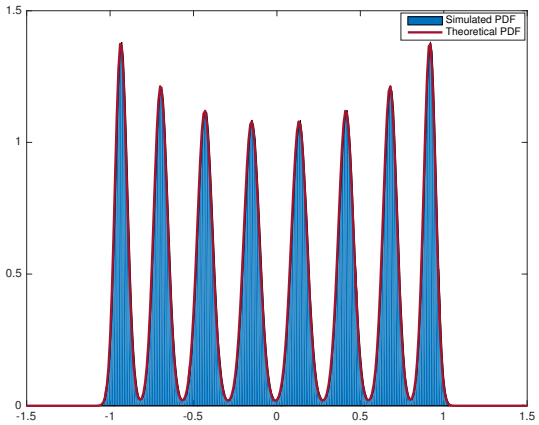

(b) $\alpha_1 = 1$, $\alpha_3 = -0.075 - 0.025j$

Figure 3.7: The theoretical and simulated pdf of 8-PAM without (a) and with (b) receiver nonlinearity at an SNR of 20 dB

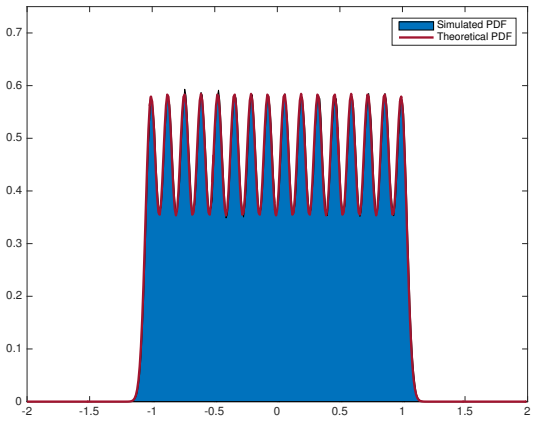

(a) Perfectly linear receiver

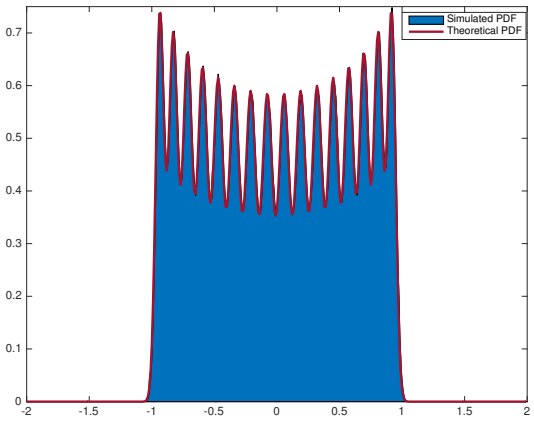

(b) $\alpha_1 = 1$, $\alpha_3 = -0.075 - 0.025j$

Figure 3.8: The theoretical and simulated pdf of 16-PAM without (a) and with (b) receiver nonlinearity at an SNR of 20 dB

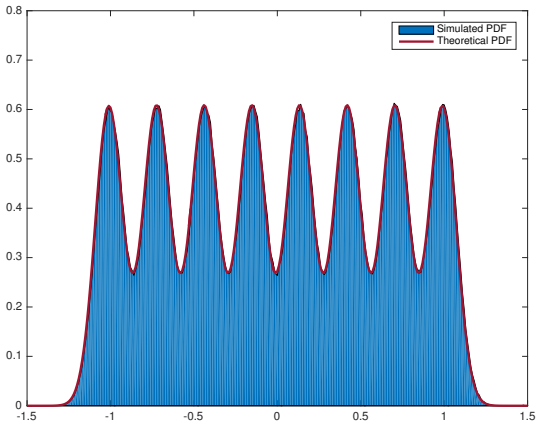

(a) Perfectly linear receiver

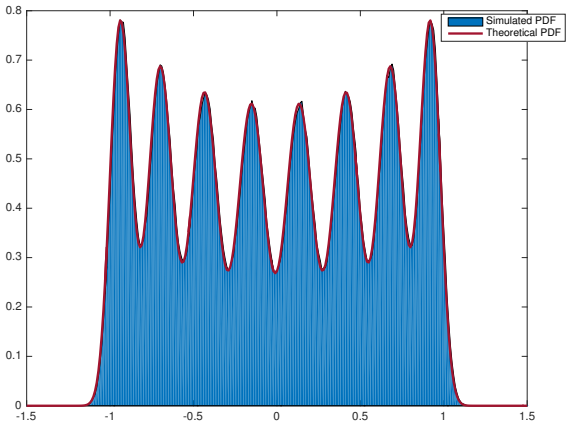

(b) $\alpha_1 = 1$, $\alpha_3 = -0.075 - 0.025j$

Figure 3.9: The theoretical and simulated pdf of 8-PAM without (a) and with (b) receiver nonlinearity at an SNR of 15 dB

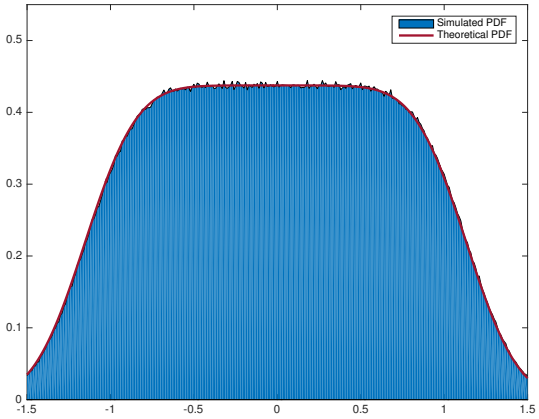

(a) Perfectly linear receiver

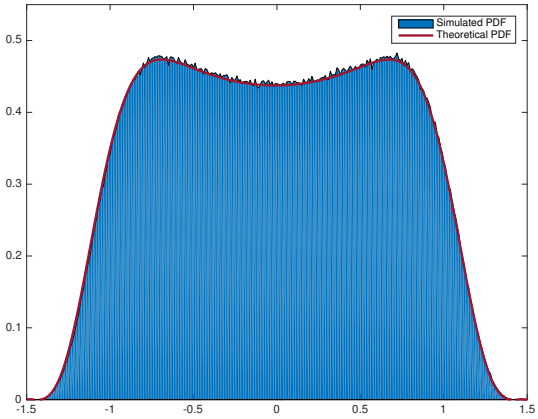

(b) $\alpha_1 = 1$, $\alpha_3 = -0.075 - 0.025j$

Figure 3.10: The theoretical and simulated pdf of 8-PAM without (a) and with (b) receiver nonlinearity at an SNR of 5 dB

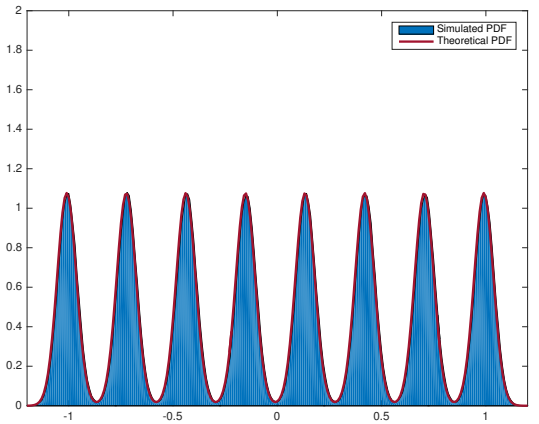

(a) Perfectly linear receiver

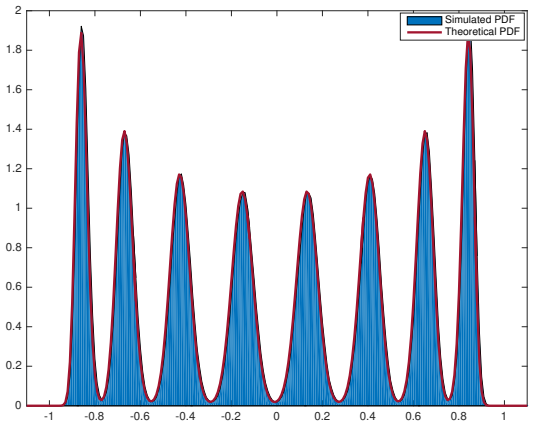

(b) $\alpha_1 = 1$, $\alpha_3 = -0.15 - 0.05j$

Figure 3.11: The theoretical and simulated pdf of 8-PAM without (a) and with (b) receiver nonlinearity at an SNR of 20 dB

To determine the validity of the M-QAM pdf expressions, the simulated and theoretical pdfs were modeled for 4-QAM and 16-QAM. The simulated pdf was found by creating a 3D histogram of the received signal averaged over 50 iterations. Figure 3.12 shows an example of these results for a 4-QAM signal with a high amount of both amplitude and phase distortion looked at from three different angles. The amplitudes of the simulated and theoretical results appear to match and both of the pdfs appear to have similar amounts of rotation for each of the symbol points. Numerical results for the accuracy of the match between the two pdfs are provided in the following section. Figures 3.13 and 3.14 show similar plots for the case of a 16-QAM signal with nonlinearity.

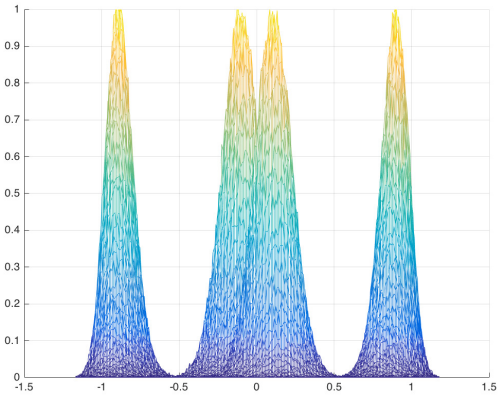

(a) Simulated pdf - front view

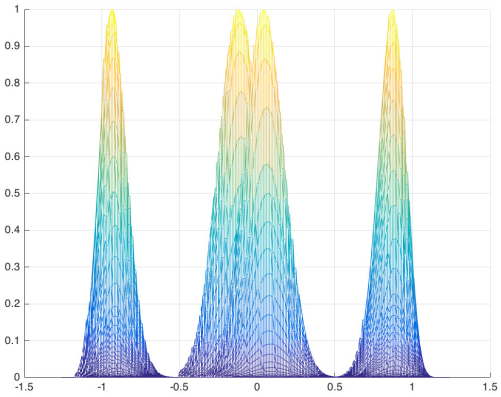

(b) Theoretical pdf - front view

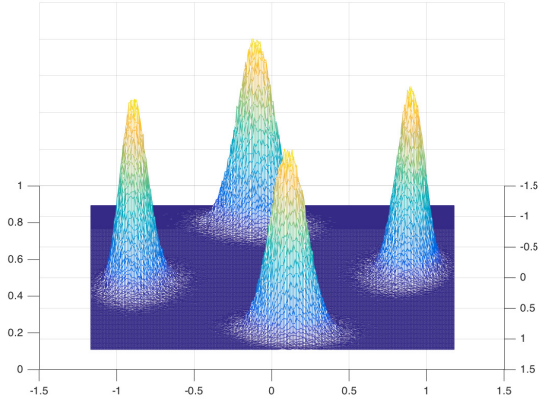

(c) Simulated pdf - side view

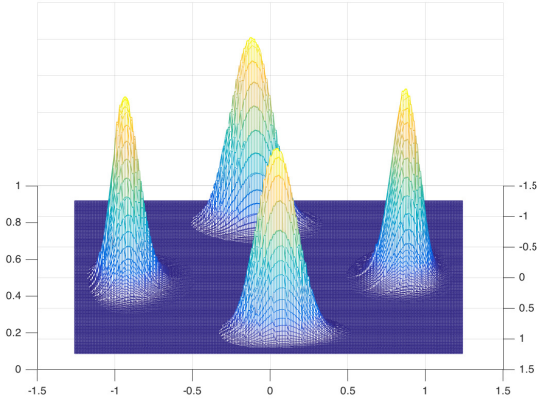

(d) Theoretical pdf - side view

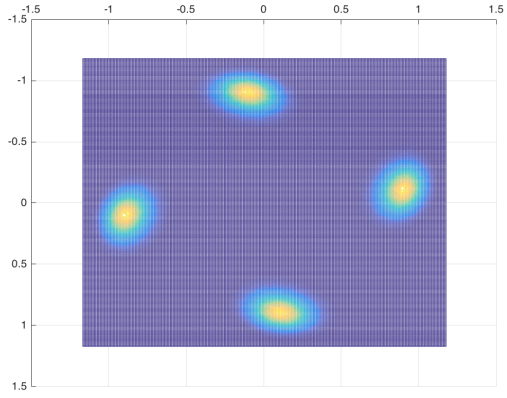

(e) Simulated pdf - top view

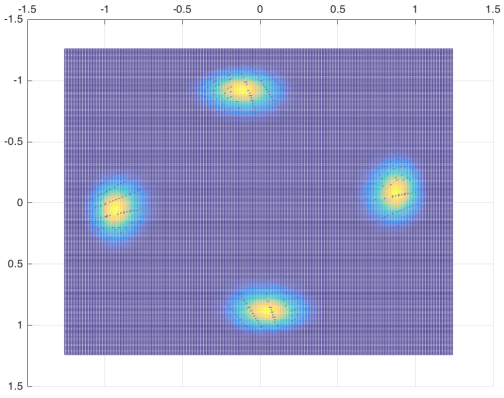

(f) Theoretical pdf - top view

Figure 3.12: The theoretical and simulated 3D pdf of a 4-QAM signal with $\alpha_1 = 1$ and $\alpha_3 = -0.1 - 0.1j$ viewed from three different angles.

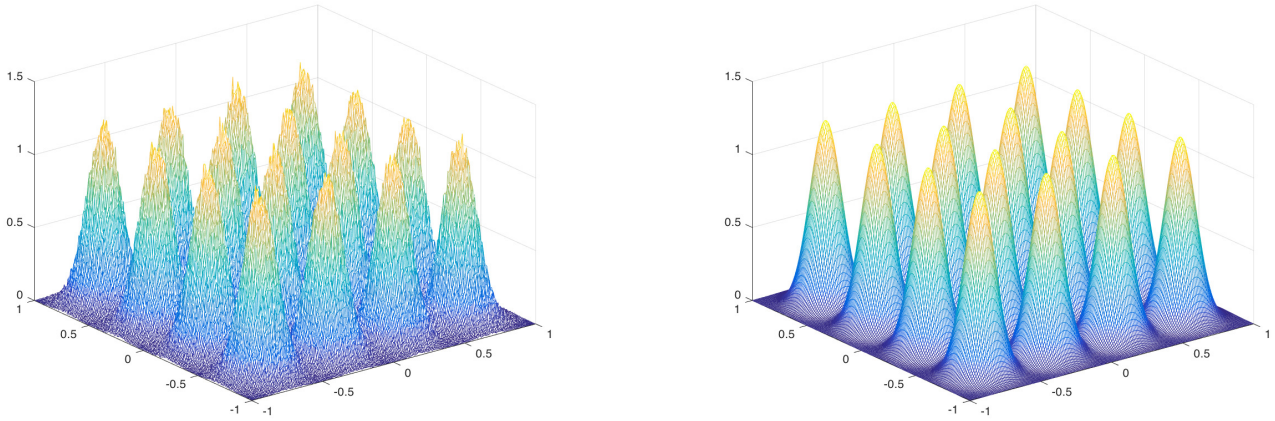

(a) Simulated pdf **(b)** Theoretical pdf

Figure 3.13: The simulated and theoretical pdfs of 16-QAM without receiver nonlinearity at an SNR of 15 dB

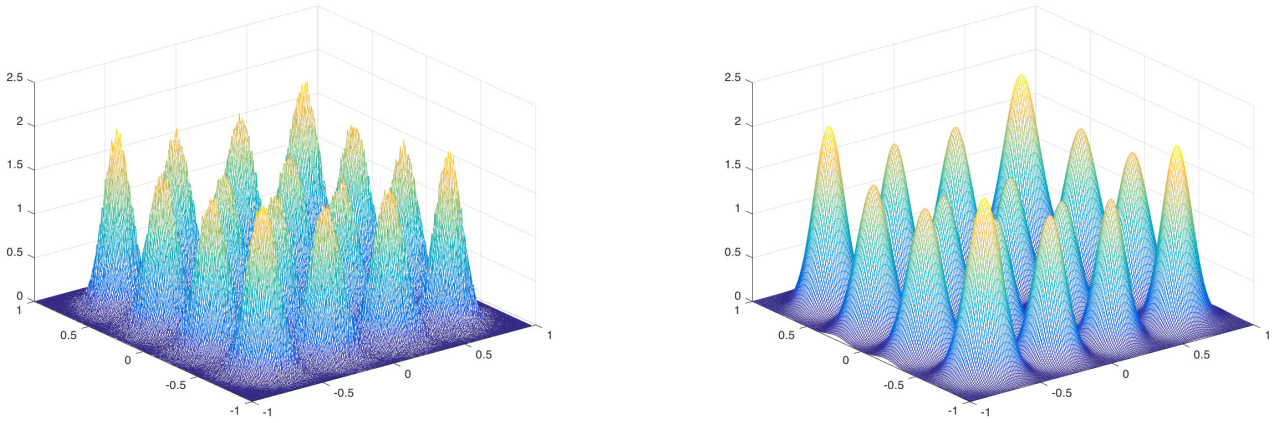

(a) Simulated pdf **(b)** Theoretical pdf

Figure 3.14: The simulated and theoretical pdfs of 16-QAM with receiver nonlinearity at an SNR of 15 dB, $\alpha_1 = 1$, $\alpha_3 = -0.06$

3.4.2 Accuracy of Theoretical Results

The mean squared error (MSE) was calculated between the theoretical and simulated pdf results across SNRs from -5 dB to 20 dB with receiver nonlinearities ranging from no nonlinearity to severe distortion to determine the accuracy of the theoretical pdf expressions. This accuracy measure was chosen because other methods such as mean percent error do not give accurate results when comparing values that are very small, such as $< 10^{-6}$. The equation for mean squared error for two vectors, where n is the length of the vectors, is:

$$\text{MSE} = \frac{1}{n}\sum_{i=1}^{n}(Y_i - X_i)^2 \tag{3.17}$$

Equation (3.17) shows how the error is calculated between a predicted series of data x and a theoretical series of data y. This error was calculated between the values of a simulated histogram modeling a signal's distribution and the theoretical pdf curve. Because the values being compared are between a histogram, which produces finite bins of data, and a theoretical curve it is expected that part of the MSE will be due to this binning error. Therefore, the MSEs with receiver nonlinearity will be compared with the MSE of no receiver nonlinearity.

For each signal tested, the MSE was calculated at SNRs from -5 dB to 20 dB in steps of 1 with 8 different degrees of receiver nonlinearity. The simulated pdf was approximated by creating a histogram for the signal, taking the maximum value from each bin, and then interpolating these values to get a smooth curve. This was averaged across 50 iterations to remove any outlying points. Then the MSE was calculated between the simulated and theoretical pdfs. For the M-QAM signals, the MSE was calculated for a projection of the

3D pdf onto the Q axis and the I axis to better compare with the M-PAM signal results.

The modulated signals tested were 2-PAM, 4-PAM, 8-PAM, 16-PAM, and 4-QAM although it is expected that the derived equations would still apply for higher order signals. Each signal was normalized to have a peak power of 1, so that the same nonlinearity coefficients would cause the same amount of distortion in each signal. The six degrees of nonlinearity chosen are shown in Table 3.1.

α_1	α_3
1	0
1	-0.075+0.025j
1	-0.05-0.1j
1	-0.1+0.02j
1	-0.125+0.05j
1	-0.15

Table 3.1: The six degrees of receiver nonlinearity used to calculate the mean squared error

These values were chosen because they provide a large range of various real-world nonlinearity situations. Some have both amplitude and phase distortion while others have either strong amplitude or strong phase distortion. An example of an 8-PAM constellation with these nonlinearity values is shown in Figure 3.15. Figure 3.16 shows 2-PAM, 8-PAM, and 16-QAM signals with the same peak power with the same nonlinearity values. The outer points in each of the signals have the same amounts of amplitude and phase distortions.

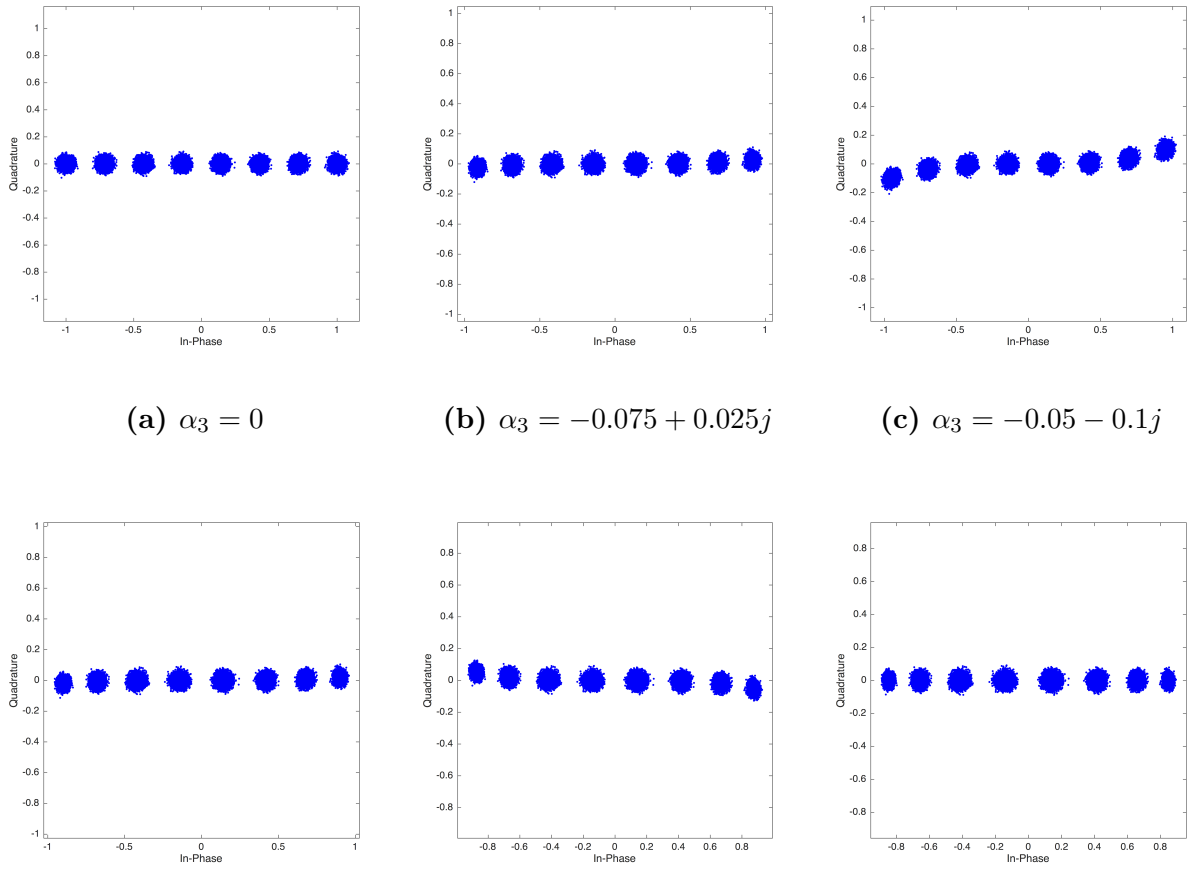

(a) $\alpha_3 = 0$ **(b)** $\alpha_3 = -0.075 + 0.025j$ **(c)** $\alpha_3 = -0.05 - 0.1j$

(d) $\alpha_3 = -0.1 + 0.02j$ **(e)** $\alpha_3 = -0.125 + 0.05j$ **(f)** $\alpha_3 = -0.15$

Figure 3.15: The six degrees of receiver nonlinearity that were tested, demonstrated with the signal constellation of an 8-PAM signal at an SNR of 25 dB with and without nonlinearity, $\alpha_1 = 1$

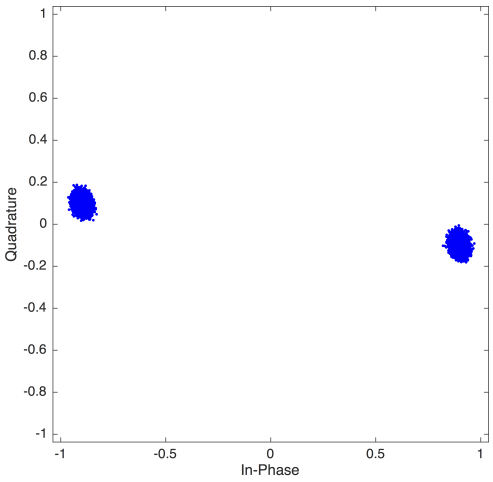

(a) 2-PAM

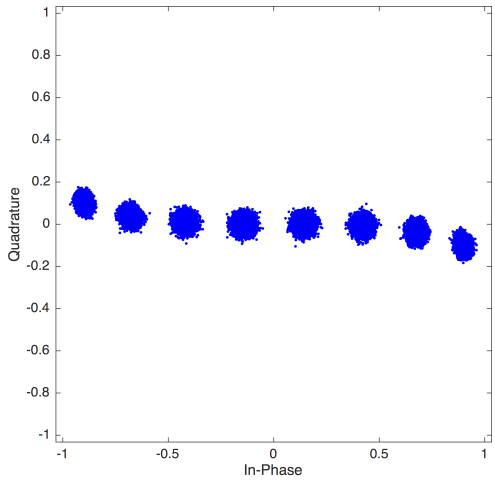

(b) 8-PAM

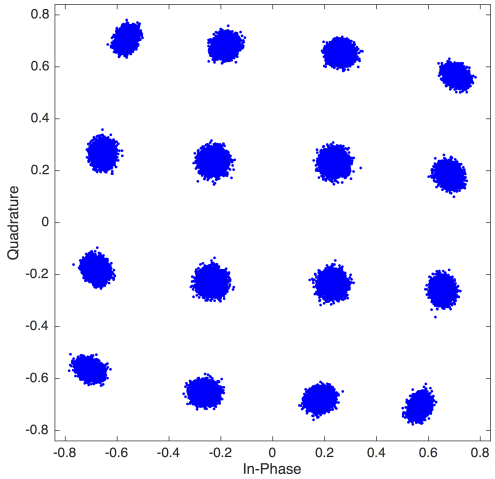

(c) 16-QAM

Figure 3.16: Three modulated signals with SNR=30 dB, peak power = 1, and $\alpha_1 = 1$, $\alpha_3 = -0.1 - 0.1j$

Figures 3.17, 3.18, 3.19, 3.20, and 3.21 show the mean squared error measurements for the tested signals for SNRs between -5 dB and 20 dB, with the simulated signal averaged over 25 iterations for the PAM signals and averaged over 50 iterations for the QAM signals. The mean squared error plots for 4-PAM, 8-PAM, and 16-PAM were almost identical - as the amount of nonlinearity increased the mean squared error increased. This increase was most dramatic at SNRs below 5 dB. At higher SNRs the nonlinear pdfs were very close in accuracy to the linear pdf. For the 2-PAM pdfs, the accuracy of the nonlinear pdfs did not approach the accuracy of the linear pdf until SNRs of around 10 dB. At lower SNRs, there was a large variation in the accuracy depending on the amount of receiver nonlinearity. Because there is less channel noise at high SNRs, the pdfs of the signals at these SNRs will be smoother than the pdfs at low SNRs for the same number of simulation iterations. Therefore, the decrease in accuracy at low SNRs is partially due to this factor, and could possibly be mitigated by increasing the number of iterations. There was also a slight decrease in accuracy at SNRs above 15 dB, which is most likely due to the binning error from the histogram. At high SNRs, the pdf at each received symbol is narrower, so each histogram bin contains more information than at lower SNRs.

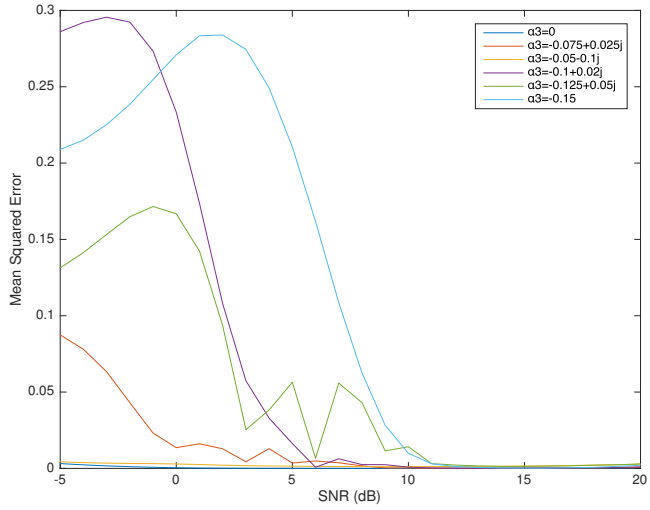

Figure 3.17: The mean squared error of a 2-PAM pdf with six levels of receiver nonlinearity across SNRs from -5 to 20 dB

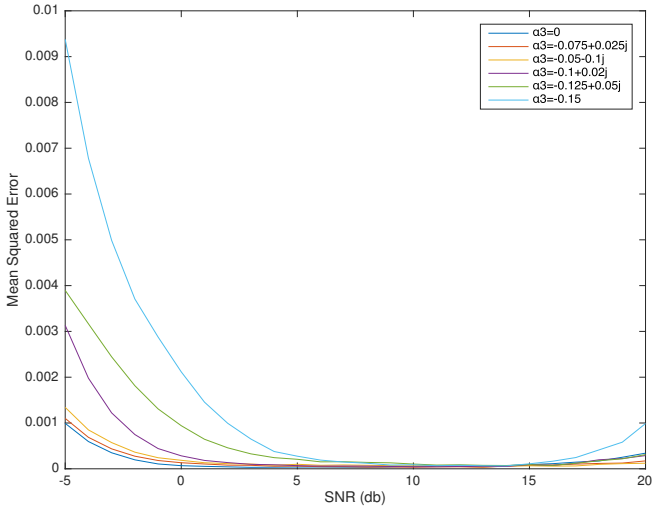

Figure 3.18: The mean squared error of an 4-PAM pdf with six levels of receiver nonlinearity across SNRs from -5 to 20 dB

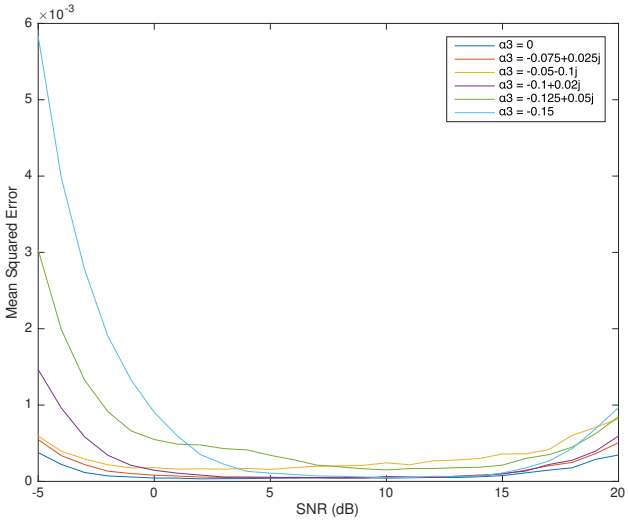

Figure 3.19: The mean squared error of an 8-PAM pdf with six levels of receiver non-linearity across SNRs from -5 to 20 dB

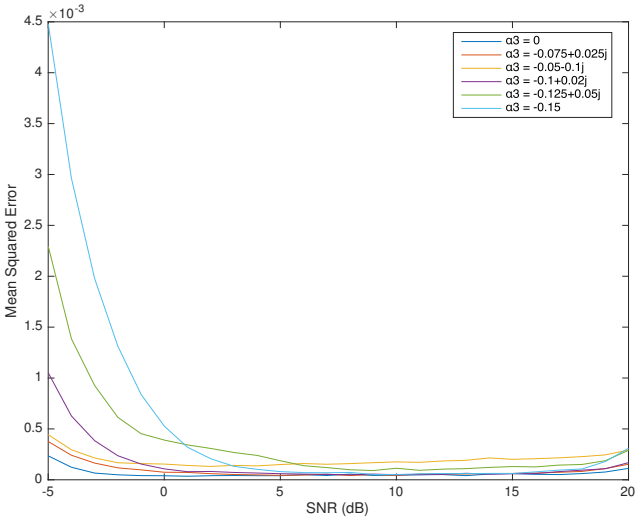

Figure 3.20: The mean squared error of a 16-PAM pdf with six levels of receiver non-linearity across SNRs from -5 to 20 dB

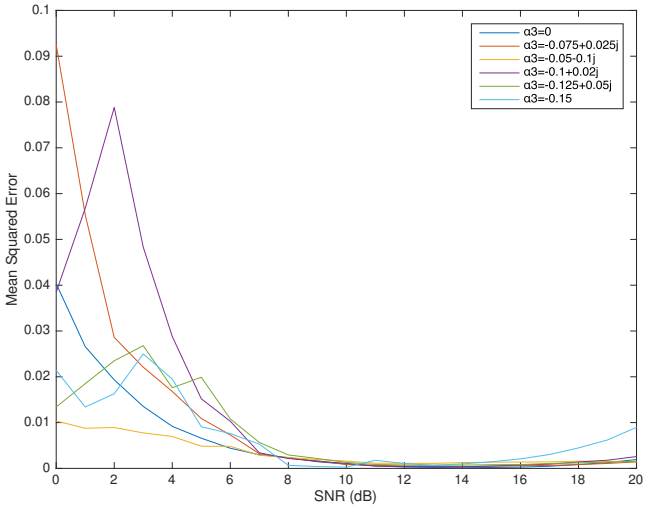

Figure 3.21: The mean squared error of a 4-QAM pdf with six levels of receiver nonlinearity across SNRs from -5 to 20 dB

3.5 Summary

The change of variables technique can be used to derive the probability density functions of amplitude modulated signals with receiver nonlinearity when the nonlinearity is modeled with a polynomial model. When the accuracy is measured with mean squared error, these derived expressions for M-PAM and rectangular M-QAM have similar accuracies to the pdf expressions for a linear receiver, especially at SNRs above 5 dB. At lower SNRs the model becomes less accurate as the amount of nonlinearity increases, but it still matches the simulated pdf fairly well and the error is most likely caused by the larger amount of noise at those SNRs. Chapter 4 describes how these expressions can be modified to account for the presence of interference and Chapter 5 describes how these expressions can be integrated to

find theoretical bit and symbol error rate expressions both with and without the presence of interference.

Chapter 4

Modeling the Probability Density Functions of M-PAM and M-QAM Signals with Nonlinear Receivers in the Presence of Interference

Blocking signals are signals at frequencies adjacent to a signal of interest that lead to a performance loss due to desensitization caused by receiver nonlinearity. This chapter analyzes the effect of a tone blocking signal, M-PAM blocking signal, and M-QAM blocking signal on the probability density functions of amplitude modulated signals. There are several assumptions that will be made for this analysis:

- The blocking signal has the same symbol period as the signal of interest
- The blocking signal and the signal of interest are unsynchronized

- The bandwidth of the desired signal and the distortion product created by the blocking signal are equal

Although in realistic channel scenarios there would not always be a complete overlap between the blocking signal and the desired signal, the same derivation process used in this analysis can be extended for the case of partial overlap.

4.1 The Effect of a Tone Blocker on the Probability Density Function

Blocking signals lead to a reduction in gain of a desired signal. This chapter will analyze the effect of one adjacent blocking signal on the probability density functions of M-PAM and M-QAM signals. The tone blocking signal $A_i \cos(2\pi f_2 t)$ will be at some frequency f_2 close to the desired signal at frequency f_1. Suppose the desired signal is $A_s \cos(2\pi f_1 t)$ making the input signal to the front end $x(t) = A_s \cos(2\pi f_1 t) + A_i \cos(2\pi f_2 t)$. Using a third order polynomial model $y(t) = \alpha_1 x(t) + \alpha_3 x^3(t)$, the total received signal at the desired frequency f_1 will become [41]:

$$y(t) = (\alpha_1 A_s + \frac{3}{4}\alpha_3 A_s^3 + \frac{3}{2}\alpha_3 A_i^2 A_s)\cos(2\pi f_1 t) \tag{4.1}$$

For simplicity, the equivalent baseband model to this expression will be used, which for an arbitrary signal of interest $s(t)$ and blocking signal $i(t)$ will become:

$$y(t) = \alpha_1 s(t) + \frac{3}{4}\alpha_3 s^2(t)s^*(t) + \frac{3}{2}\alpha_3 i^2(t)s^*(t) \tag{4.2}$$

When the blocker is unmodulated and is a constant tone of amplitude A_i with a phase shift of ϕ with respect to the signal of interest, the received amplitude will become $A_i e^{j\phi} = A_i \cos(\phi) + jA_i \sin(\phi)$. The square of this amplitude would be $A_i(\cos(\phi) - \sin(\phi)) + jA_i(\sin(\phi) + \cos(\phi))$. Therefore, the received signal $y(t)$ taking nonlinearity and this phase difference into account will be:

$$y(t) = \alpha_1 s(t) + \frac{3}{4}\alpha_3 s^2(t)s^*(t) + \frac{3}{2}\alpha_3(A_i(\cos(\phi) - \sin(\phi)) + jA_i(\sin(\phi) + \cos(\phi)))s^*(t) \quad (4.3)$$

The second term will lead to a reduction in amplitude of the desired signal as the amplitude of the blocking signal increases. The interfering signal is capable of reducing the gain of the signal of interest to zero, completely blocking it. When the signal of interest is M-PAM modulated, the probability density function will be modified to take the term from the interferer into account. Only considering a third order polynomial model, the pdf will be expressed as:

$$f_y(y) = \frac{1}{\mathrm{M}\left|\alpha_1 + \frac{3}{2}\alpha_3(A_i e^{j\phi})^2 + \frac{9}{4}\alpha_3(g^{-1}(y))^2\right|} \sum_{m=1}^{\mathrm{M}} \frac{1}{\sqrt{2\pi\sigma^2}} e^{\frac{-(g^{-1}(y)-x_m)^2}{2\sigma^2}} \quad (4.4)$$

Figure 4.1 shows the effect of the tone blocker on the pdf of a 4-PAM signal. As the power of the blocker increases, the symbols move closer to each other and decrease in power.

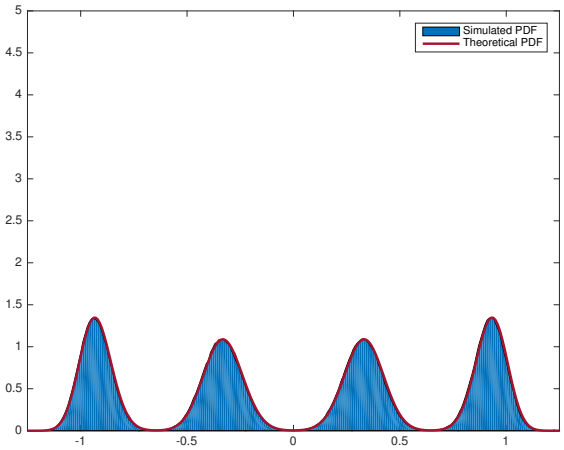

(a) The pdf without tone interference

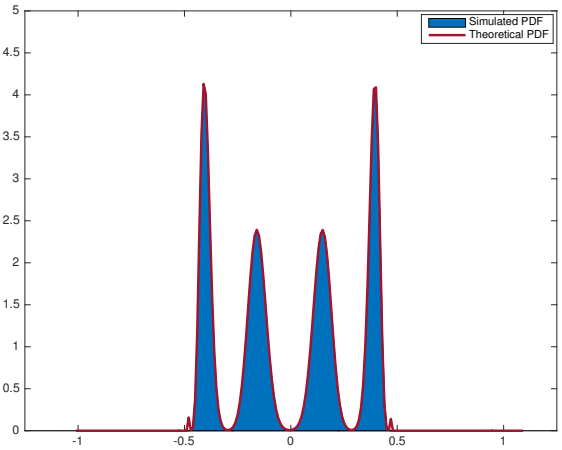

(b) The pdf with tone interference $A_i = 2.25$

Figure 4.1: The pdf of a 4-PAM signal with receiver nonlinearity and without (a) and with (b) a tone blocking signal. The SNR=15 dB and $\alpha_1 = 1$ and $\alpha_3 = -0.07$

The pdf for an M-QAM signal is modified in a similar way to M-PAM in the presence of a tone blocker. Adding the blocking term to the pdf derived in Chapter 3 leads to:

$$f_{x',y'}(x',y') = \frac{1}{M\left|\alpha_1 + \frac{3}{2}\alpha_3(A_i e^{j\phi})^2 + \frac{9}{4}\alpha_3(g^{-1}(x'))^2\right| * \left|\alpha_1 + \frac{3}{2}\alpha_3(A_i e^{j\phi})^2 + \frac{9}{4}\alpha_3(g^{-1}(y'))^2\right|} * \sum_{k=1}^{\sqrt{M}}\sum_{l=1}^{\sqrt{M}} \frac{1}{2\pi\sigma^2} e^{\frac{-((g^{-1}(x')-x_k)^2+(g^{-1}(y')-y_l))^2}{2\sigma^2}} \tag{4.5}$$

4.2 The Effect of an M-PAM Modulated Blocker on the Probability Density Function

An M-PAM modulated blocking signal will introduce amplitude modulation to the signal of interest. This phenomenon is known as cross-modulation, and it can be a significant detriment to amplitude modulated signals for high powered blockers. The first case considered will be the case of a 2-PAM modulated interfering signal with amplitudes $\pm A_i e^{j\phi}$. Because the interference term in the output expression is squared, this effect on the pdf of the desired signal will be the same as the case of the tone blocker but with interference amplitude of $\sqrt{A_i e^{j\phi}}$. However, for higher modulation order, the additional amplitude distortion becomes apparent in the received signal. A 4-PAM blocker with amplitude levels $(\pm A_i e^{j\phi}, \pm\frac{A_i e^{j\phi}}{3})$ will become a two-level amplitude modulated signal with levels $(A_i e^{j\phi}, \frac{A_i e^{j\phi}}{3})$ after being squared and added to the signal of interest according to (4.2). This will lead to twice the number of exponential terms in the resulting pdf because each term corresponding to a symbol in the desired signal will be added with each of the two levels for the blocking signal. Letting $f_x(x)$ denote the linear pdf of the M-PAM signal, and $g_1(x)$ and $g_2(x)$ as follows:

$$g_1(x) = (\alpha_1 + \frac{3}{2}\alpha_3 A_i e^{j\phi})x + \alpha_3 x^3 \tag{4.6}$$

$$g_2(x) = (\alpha_1 + \frac{3}{2}\alpha_3 \frac{A_i e^{j\phi}}{9})x + \alpha_3 x^3 \tag{4.7}$$

The pdf for an M-PAM signal with a 4-PAM blocker will be modified to become:

$$f_y(y) = f_x(g_1^{-1}(y)) \left| \frac{\partial}{\partial y} g_1^{-1}(y) \right| + f_x(g_2^{-1}(y)) \left| \frac{\partial}{\partial y} g_2^{-1}(y) \right| \tag{4.8}$$

For the general case where the blocking signal is M-PAM with positive amplitude levels A_m, $m = 1, 2, ..., M/2$, let $g_m(x)$ be:

$$g_m(x) = (\alpha_1 + \frac{3}{2}\alpha_3(A_m e^{j\phi})^2)x + \alpha_3 x^3 \tag{4.9}$$

Using this $g_m(x)$ equation, the pdf for an M-PAM signal with an M-PAM blocker will be:

$$f_y(y) = \sum_{m=1}^{M/2} f_x(g_m^{-1}(y)) \left| \frac{\partial}{\partial y} g_m^{-1}(y) \right| \tag{4.10}$$

Figure 4.2 shows the simulated and theoretical pdf of a 2-PAM signal with 4-PAM blockers following (4.10). The simulated and theoretical plots overlap, and each received symbol has two peaks corresponding to the two amplitude levels caused by the blocking signal. The additional amplitude modulation is very apparent when the blocker has a power greater than the power of the signal of interest and there is nonlinearity present.

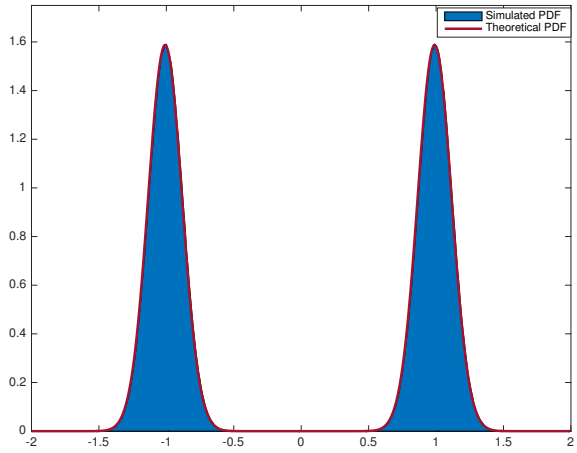

(a) The simulated pdf with a linear receiver

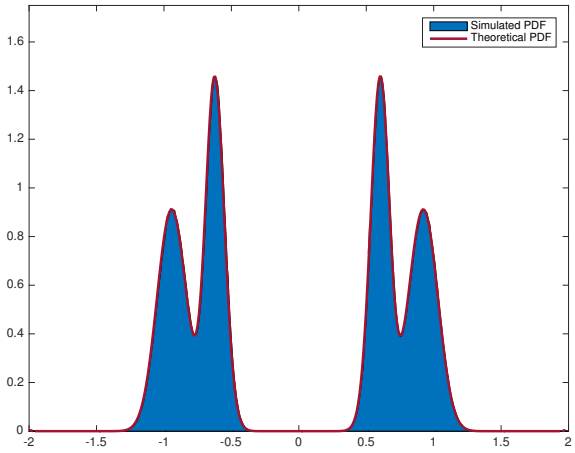

(b) The theoretical pdf with $\alpha_1 = 1$ and $\alpha_3 = -0.03$

Figure 4.2: The pdf of a 2-PAM signal with 4-PAM interference amplitude levels $[\pm\sqrt{8}, \pm\frac{\sqrt{8}}{3}]$, SNR=15 dB

For M-QAM with M-PAM blockers, the pdf will follow (4.10) except the 3D pdf for the linear QAM signal $f_{x',y'}(x', y')$ will be used in place of $f_x(x)$, making the nonlinear pdf:

$$f_{x',y'}(x', y') = \sum_{m=1}^{M/2} f_{x',y'}(g_m^{-1}(x'), g_m^{-1}(y')) \left| \frac{\partial}{\partial x'} g_m^{-1}(x') \right| \left| \frac{\partial}{\partial y'} g_m^{-1}(y') \right| \tag{4.11}$$

where the g_m are given in (4.9).

4.3 The Effect of an M-QAM Modulated Blocker on the Probability Density Function

An M-QAM blocking signal will add distortion to both the I and the Q axes of the desired signal. For the simplest case of 4-QAM, a 4-QAM signal with amplitudes $\{-A_i - jA_i,$

$-A_i + jA_i,\ A_i - jA_i,\ A_i + jA_i\}$ will become a 2 level signal with amplitudes $\{\pm 2jA_i^2\ \}$ when squared. When this signal interferes with the desired signal, amplitude modulation will occur along the I axis. Like the M-PAM blocker case, let $g_m(z)$ be:

$$g_m(z) = (\alpha_1 + \frac{3}{2}\alpha_3(A_m e^{j\phi})^2)z + \alpha_3 z^3 \tag{4.12}$$

where A_m is each of the M complex amplitudes of the M-QAM signal and z is a complex signal. Because of the symmetry of a rectangular M-QAM constellation, there will be $m = \frac{M}{2}$ possible solutions to (4.12). Because the distortion from this blocker will occur along the I and the Q axes, both an M-PAM and an M-QAM signal of interest will be represented by their 3-D pdf. Let $f_{x,y}(x, y)$ denote the 3-D pdf for either an M-PAM or M-QAM signal of interest. The nonlinear pdf with the M-QAM blocker will therefore be:

$$f_{x',y'}(x', y') = \sum_{m=1}^{M/2} f_{x',y'}(g_m^{-1}(x'), g_m^{-1}(y')) \left|\frac{\partial}{\partial x'} g_m^{-1}(x')\right| \left|\frac{\partial}{\partial y'} g_m^{-1}(y')\right| \tag{4.13}$$

Figure 4.7 shows the theoretical and simulated pdf of a 2-PAM signal with a 4-QAM blocker with a mild amount of receiver nonlinearity.

4.4 Results

The mean squared error was used to measure the accuracy of the theoretical M-PAM pdf expressions for a range of SNRs and powers of the blocking signals. Because the M-QAM interfering signals introduced distortions along the imaginary and real axes of the pdf, qualitative results are better able to show the accuracy of the expressions. Chapter 3 demonstrated

the accuracy of the theoretical expressions as a function of the amount of nonlinearity, so the amount of receiver nonlinearity was held constant at a moderate amount of nonlinearity for these calculations. The scenarios considered were 4-PAM and 4-QAM signals with an adjacent tone blocker, 4-PAM and 4-QAM signals with a 4-PAM blocker, and a 2-PAM with a 4-QAM blocker. The signals of interest had peak powers of 1. The 4-PAM signal had amplitude levels $\{\pm 1, \pm\frac{1}{3}\}$ and the 4-QAM signal had amplitude levels $\{\pm\frac{\sqrt{2}}{2} \pm j\frac{\sqrt{2}}{2}\}$.

4.4.1 Tone Blocker PDF Accuracy

Figure 4.3 shows the mean squared error for a 4-PAM signal with a tone blocker. Five different power levels of the tone were tested, and the MSE was calculated for SNRs between -5 and 20 dB in steps of 1. For the MSE calculation, the simulated pdf was averaged over 25 iterations to produce a smooth curve. Like the results from Chapter 3 for the MSE for nonlinearity without blockers, the accuracy of the blockers matches the accuracy of the no blocker case very well at high SNRs, with a decrease in accuracy at low SNRs, and a slight decrease at SNRs above 15 dB. At low SNRs, the accuracy decreased as the power of the blocker increased. However, at SNRs greater than 0 dB, the accuracy is high for all of the power levels tested and the accuracy of the pdfs with the blocker does not differ significantly from the accuracy of the pdfs without a blocker. The decrease in accuracy at the higher SNRs tested is again most likely due to the the narrowing of the pdf at high SNRs, which makes each histogram bin less accurate in representing the actual pdf.

Figure 4.4 shows the theoretical and simulated 3D pdf of a 4-QAM signal with a tone

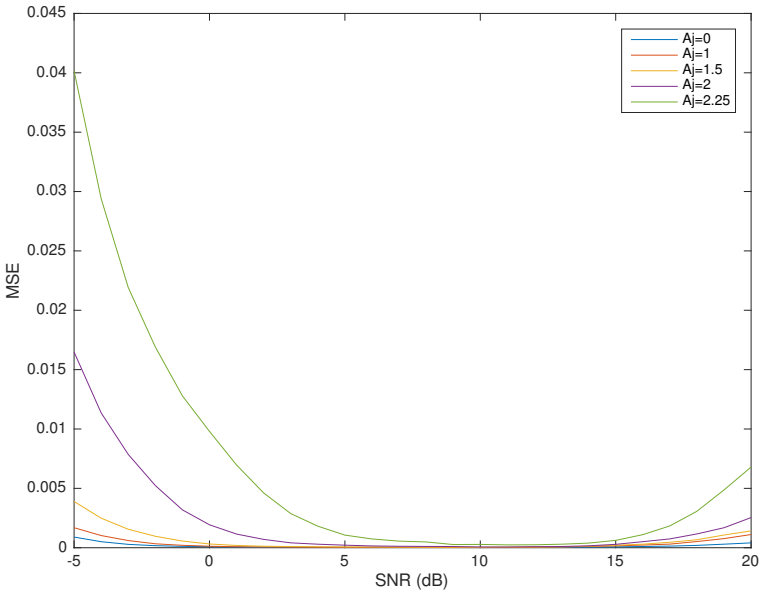

Figure 4.3: The mean squared error of a 4-PAM pdf with SNRs from -5 to 20 dB with 5 tone blocker amplitudes. $\alpha_1 = 1$ and $\alpha_3 = -0.07$

blocker from three different viewing angles. The side views of both the simulated and the theoretical pdfs match very closely, with the only difference being the slight noisiness of the simulated pdf. However, the top view shows that the actual pdf has slightly more amplitude compression than the theoretical pdf, but the difference is very minor.

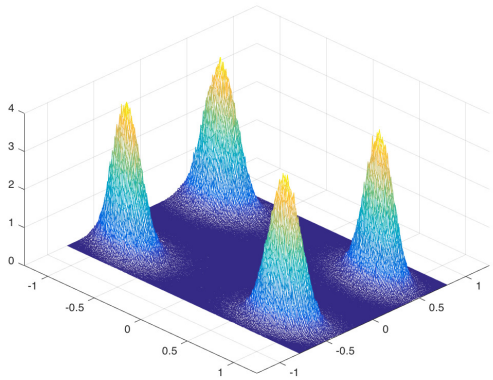

(a) Simulated pdf

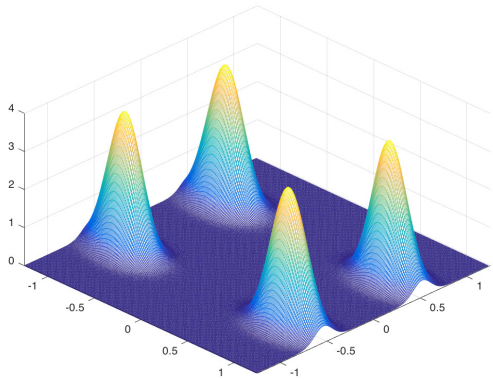

(b) Theoretical pdf

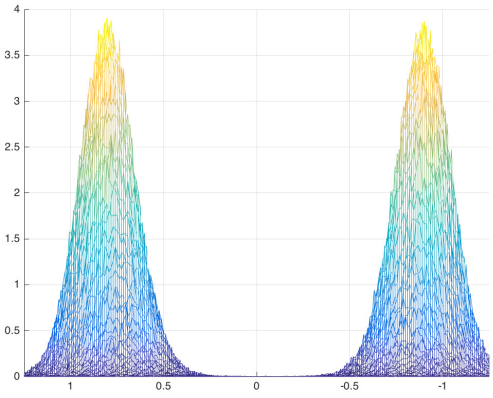

(c) Simulated pdf - side view

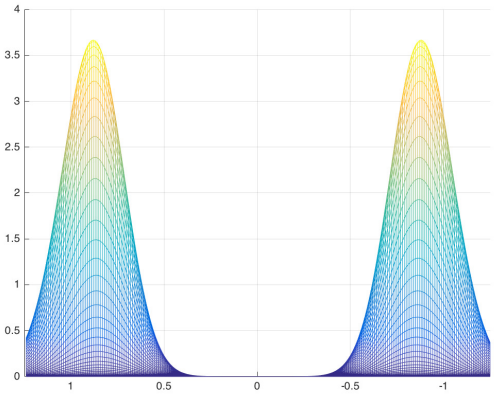

(d) Theoretical pdf - side view

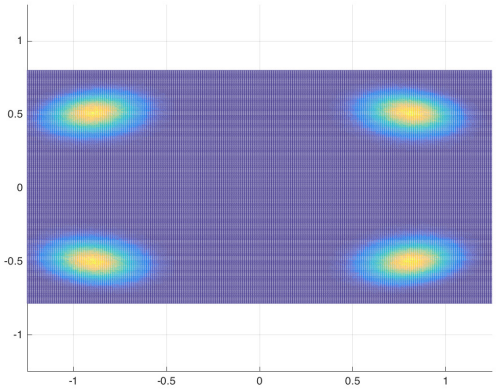

(e) Simulated pdf - top view

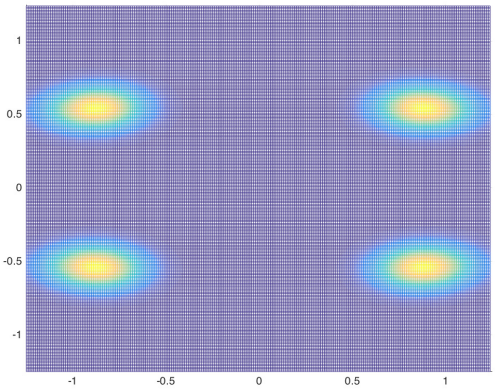

(f) Theoretical pdf - top view

Figure 4.4: The theoretical and simulated 3D pdf of a 4-QAM signal with tone interference $A_i = 1.5$ with $\alpha_1 = 1$ and $\alpha_3 = -0.07$ for three different viewing angles.

4.4.2 M-PAM Blocker PDF Accuracy

Figure 4.5 shows the mean squared error of a 4-PAM signal with a 4-PAM blocker across SNRs from -5 to 20 dB and with varying blocker power levels. As the power of the blocker increases, the accuracy of the pdf decreases at SNRs below 5 dB, but at higher SNRs the pdfs have similar accuracies for each of the tested power levels. This follows the same pattern seen in the mean squared error plots for the receiver nonlinearity without interference cases and for the nonlinearity with a tone blocker case.

Figure 4.6 shows the theoretical and simulated 3D pdf of a 4-QAM signal with 4-PAM interference of amplitudes $\{\pm 1.833, \pm 5.5\}$ at three different viewing angles. The theoretical and simulated match quite well except the simulated pdf is slightly wider along the imaginary axis than the theoretical pdf, which can be seen from the first angle. However, this is a very slight difference and would cause minor impact on the error rate expressions that can be derived from this pdf. A possible explanation for this effect is simulation inaccuracies when calculating the inverse of a complex number.

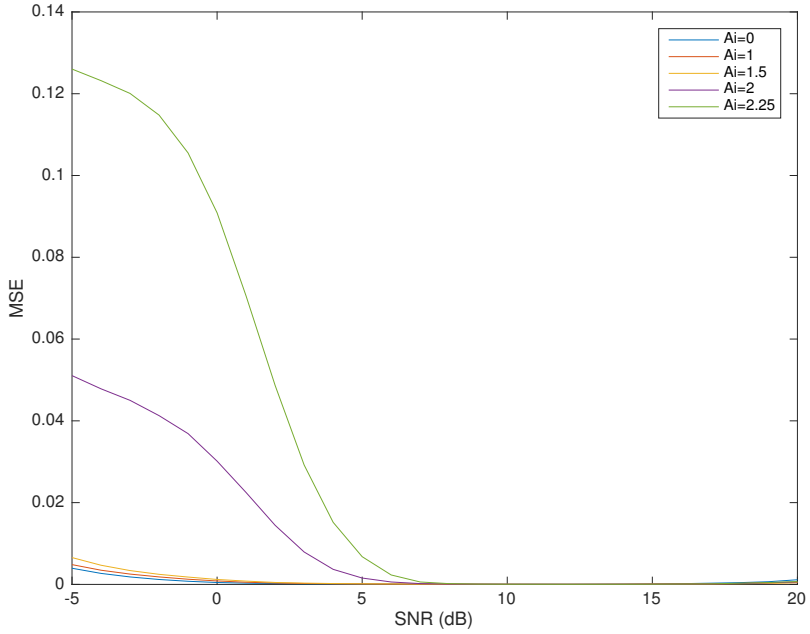

Figure 4.5: The mean squared error of a 4-PAM pdf with a 4-PAM blocker from -5 to 20 dB with 5 blocker peak amplitudes. $\alpha_1 = 1$ and $\alpha_3 = -0.07$

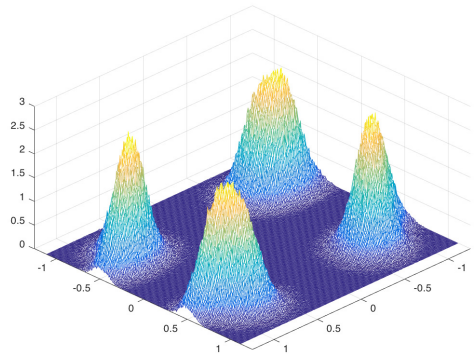

(a) Simulated pdf

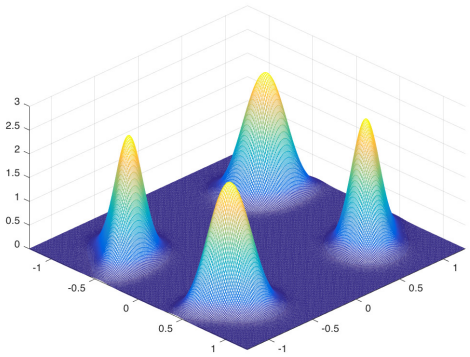

(b) Theoretical pdf

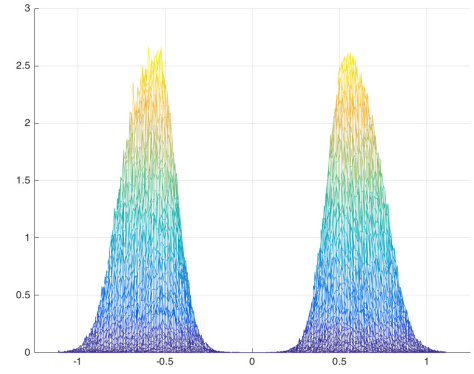

(c) Simulated pdf - side view

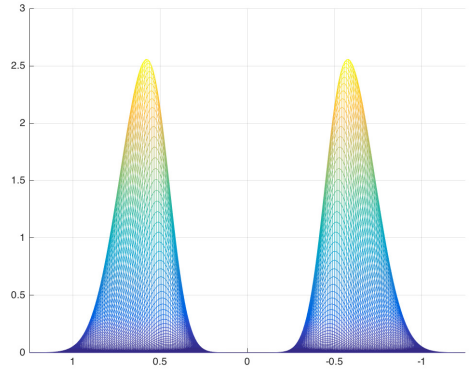

(d) Theoretical pdf - side view

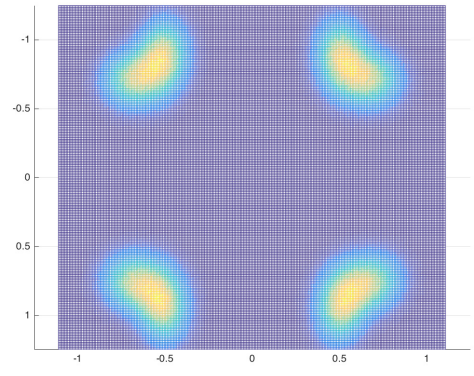

(e) Simulated pdf - top view

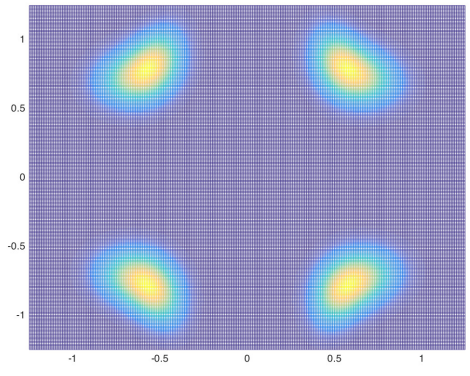

(f) Theoretical pdf - top view

Figure 4.6: The theoretical and simulated 3D pdf of a 4-QAM signal with 4-PAM interference $A_i = 5.5$ with $\alpha_1 = 1$, $\alpha_3 = -0.03$, and SNR=15dB for three different viewing angles.

4.4.3 M-QAM Blocker PDF Accuracy

Figure 4.7 shows the theoretical and simulated pdf for a 2-PAM signal with a strong 4-QAM blocker. The simulated and theoretical pdfs match almost exactly, the only difference is due to the noise caused by simulation. The 4-QAM blocking signal has caused the pdf of the 2-PAM signal to change from a circular 3-D Gaussian distribution centered at the symbol locations -1 and +1, to a pdf distorted along the imaginary axis. However, this blocker would have a low impact on the resulting symbol error rate because the symbols do not move much closer to each other due to the interference.

Overall, the pdf expressions modified to account for tone and amplitude modulated blocking signals due to nonlinearity have similar accuracy to the expressions derived in Chapter 3 for the case of receiver nonlinearity with no interference. While the distributions were slightly less accurate at very low SNRs, they had high accuracy at higher SNRs, even for the highly nonlinear cases. The expressions taking into account the blockers were slightly more accurate for the M-PAM signals of interest than the M-QAM signals of interest. Because the inaccuracies were along the imaginary axis, a possible source of error could be a miscalculation of the inverse for complex numbers. However, the difference is minor and still provides a good approximation of the pdf distortion caused by the interference.

4.5 Summary

The change of variables technique is a valid method for deriving the probability density functions of amplitude modulated signals with adjacent blocking signals. These blocking signals are a significant problem in nonlinear receivers because they desensitize the signal of interest and can completely overpower them. As the RF spectrum becomes more crowded this problem will become more significant. There will be a greater chance of a high powered signal at a close frequency not being filtered out at the receiver, which is why accurate modeling without the need for time consuming simulation is important for wireless system design. The expressions derived in this chapter were shown to be highly accurate at high SNRs across a range of blocker powers, and slightly less accurate at a lower SNR range. These expressions will be used to find theoretical bit and symbol error rates in Chapter 5.

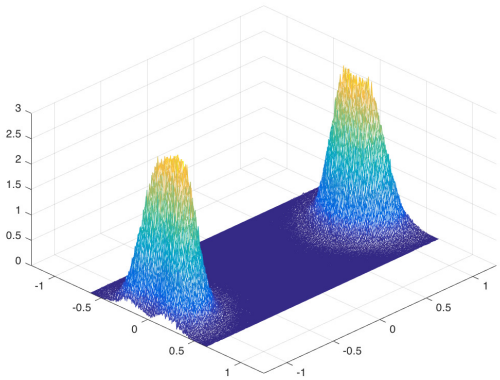

(a) Simulated pdf

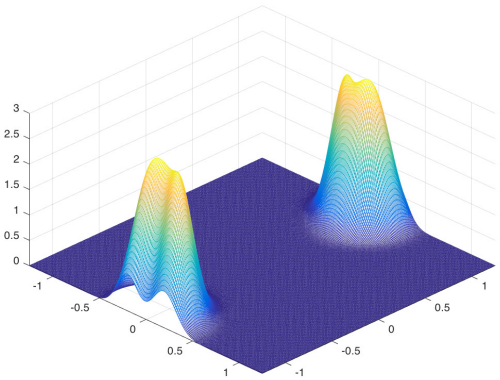

(b) Theoretical pdf

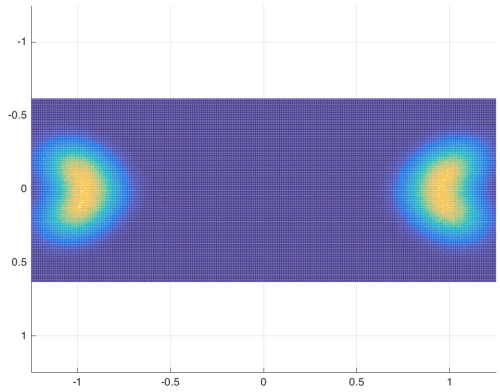

(c) Simulated pdf - side view

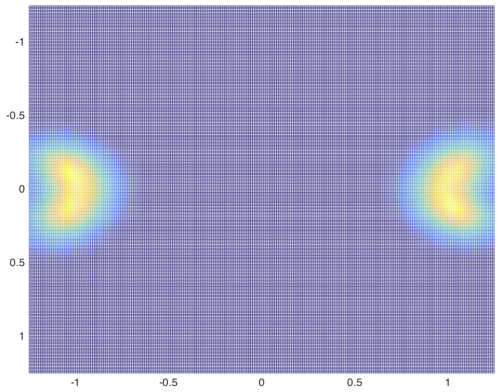

(d) Theoretical pdf - side view

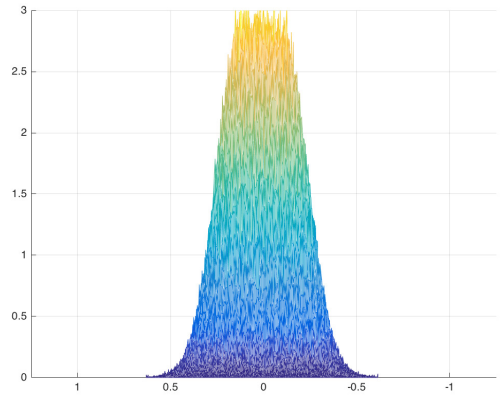

(e) Simulated pdf - top view

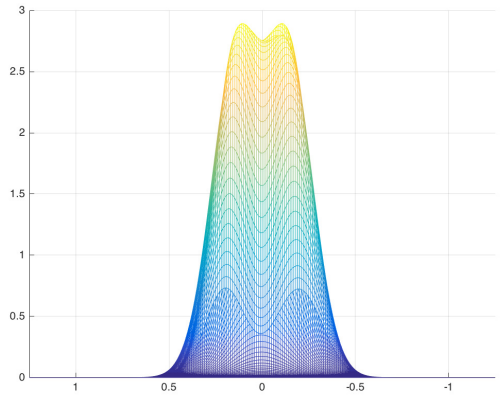

(f) Theoretical pdf - top view

Figure 4.7: The theoretical and simulated 3D pdf of a 2-PAM signal with a 4-QAM blocker $A_i = \sqrt{\frac{3}{2}}$ with $\alpha_1 = 1$, $\alpha_3 = -0.03$, and SNR=15 dB

Chapter 5

The Bit and Symbol Error Rates for M-PAM and M-QAM Signals with Nonlinear Receivers with and without the Presence of Interference

Once the probability density function has been found for a signal, the theoretical bit and symbol error rates can be derived. This chapter discusses the derivation of these rates and derives expressions for the error rates of M-PAM and M-QAM signals using the pdf expressions from Chapter 3. Then these concepts will be extended for the case where adjacent blocking signals have impacted the desired signal, and theoretical pdfs and error rates will be derived when these are tones, PAM modulated signals, or QAM modulated signals.

5.1 Bit and Symbol Error Rate Expressions for M-PAM and M-QAM Signals with Receiver Nonlinearity

The theoretical probability density functions derived in Chapter 3 for receiver nonlinearity can be used to generate symbol and bit error rate expressions. For PAM and rectangular QAM signals assuming equal likelihood of each symbol, these are found by integrating the probability density functions at the decision boundaries, which are equidistant between each symbol point. Figure 5.1 shows examples of these decision boundaries for an 8-PAM and a 4-QAM signal. Because the goal of deriving the error rate expressions is to measure the effect of receiver nonlinearity on performance, these decision boundaries will be the same as for the perfectly linear case. However, one way to mitigate the impact of receiver nonlinearity if the amount of nonlinearity is known would be to calculate the nonlinear decision boundaries and then integrate in these regions.

5.1.1 Bit and Symbol Error Rates for M-PAM

For M-PAM, the decision boundaries will be vertical lines exactly halfway between each symbol point. A symbol error occurs when the received symbol falls outside of this region. Therefore for each symbol, the probability density function will be integrated from -∞ to the decision point to the left of the symbol, and then from the decision point to the right of the symbol to +∞. The pdf at each symbol point x_k, which is one of $(2i - \mathrm{M} - 1)\sqrt{E_b/E_{av}}$,

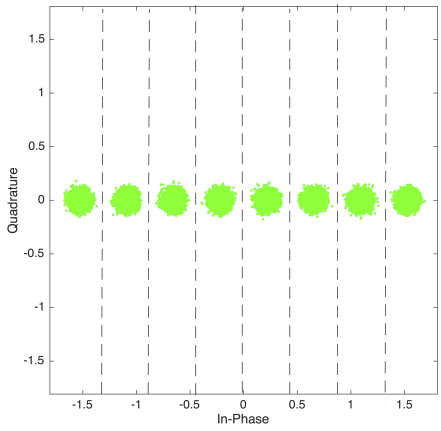

(a) Decision regions for an 8-PAM signal

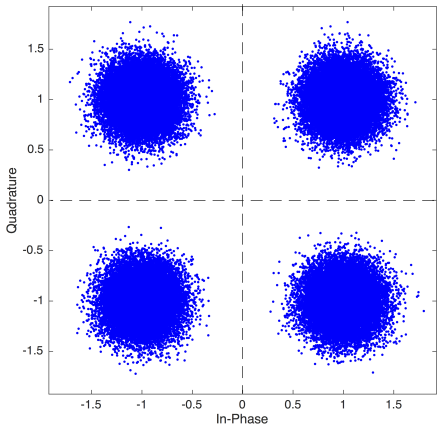

(b) Decision regions for a 4-QAM signal

Figure 5.1: Examples of the decision boundaries used to calculate the error rate, both examples have AWGN added

will be:

$$f_y(y) = \frac{1}{|\alpha_1 + 3\alpha_3(g^{-1}(x,y))^2|} \frac{1}{\sqrt{\pi N_0}} e^{\frac{-(g^{-1}(y)-x_k)^2}{N_0}} \tag{5.1}$$

Therefore, the symbol error probability of this symbol with decision boundary d_l on the left and d_r on the right will be:

$$\begin{aligned} \mathrm{P}(\text{error}|x_k) = \frac{1}{\sqrt{\pi N_0}} \Bigg(\int_{-\infty}^{d_l} \frac{1}{|\alpha_1 + 3\alpha_3(g^{-1}(x,y))^2|} e^{\frac{-(g^{-1}(y)-x_k)^2}{N_0}} dy + \\ \int_{d_r}^{\infty} \frac{1}{|\alpha_1 + 3\alpha_3(g^{-1}(x,y))^2|} e^{\frac{-(g^{-1}(y)-x_k)^2}{N_0}} dy \Bigg) \end{aligned} \tag{5.2}$$

The total symbol error probability can be found by adding up the error probabilities of each symbol, and then dividing by the total number of symbols. For example, a 4-PAM signal

with symbols at locations $\{\pm\frac{1}{3}, \pm 1\}$ would have a total symbol error rate of:

$$\mathrm{P(error)} = \frac{1}{\sqrt{\pi N_0}}\left(\frac{1}{2}\int_{-\frac{2}{3}}^{\infty}\frac{1}{|\alpha_1 + 3\alpha_3(g^{-1}(x,y))^2|}e^{\frac{-(g^{-1}(y)+1)^2}{N_0}}dy + \right.$$
$$\left.\frac{1}{2}\left(\int_{-\infty}^{-\frac{2}{3}}\frac{1}{|\alpha_1 + 3\alpha_3(g^{-1}(x,y))^2|}e^{\frac{-(g^{-1}(y)+\frac{1}{3})^2}{N_0}}dy + \int_{0}^{\infty}\frac{1}{|\alpha_1 + 3\alpha_3(g^{-1}(x,y))^2|}e^{\frac{-(g^{-1}(y)+\frac{1}{3})^2}{N_0}}dy\right)\right)$$

Because the signal constellation is symmetric, the symbol error rate can be calculated for half of the constellation and then doubled to find the total probability of symbol error. For the case where the symbols are Gray coded, which minimizes the bit error rate by coding adjacent symbols to differ from each other by one bit, the probability of bit error would be approximately $\frac{1}{log_2 M}$ multiplied by the symbol error rate.

5.1.2 Bit and Symbol Error Rates for M-QAM

For rectangular M-QAM the decision regions will be rectangular regions around each symbol point, as shown in Figure 5.1. Suppose the corner points of the rectangular decision region around a symbol s are as shown in Figure 5.2. For the symbols at the edges of the constellation, some of these decision region points might be at $\pm\infty$. Then the probability that the symbol is correct decoded would be:

$$\mathrm{P(correct|s)} = \mathrm{P}(x < c_2, x > c_1|s)\mathrm{P}(y > c_2, y < c_3|s) \tag{5.3}$$

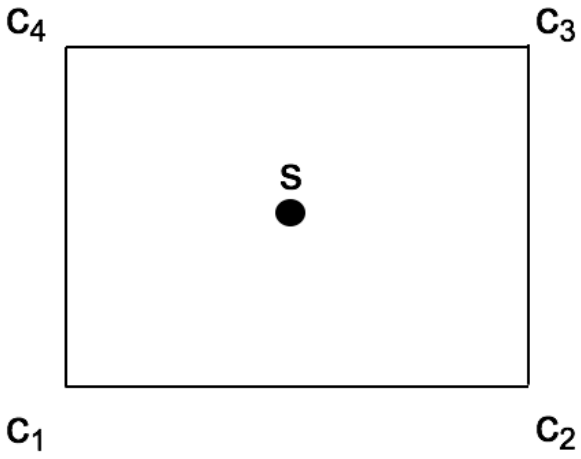

Figure 5.2: The rectangular decision region around an M-QAM symbol s

where x and y are the real and imaginary received values respectively. Therefore, the probability of an error would be 1− P(correct). The probability density of each M-QAM symbol with a linear receiver can be represented by the bivariate normal distribution:

$$f(x,y) = \frac{1}{\pi N_0} e^{-\frac{1}{N_0}((x-\Re(s))^2+(y-\Im(s))^2)} \tag{5.4}$$

where $\Re(s)$ is the real part of the symbol and $\Im(s)$ is the imaginary part. The probability that the symbol s_k will be received in error will therefore be:

$$\mathrm{P(error|s}_k) = 1 - \int_{c_2}^{c_3}\int_{c_1}^{c_2} \frac{1}{\pi N_0} e^{-\frac{1}{N_0}((x-\Re(s_k))^2+(y-\Im(s_k))^2)} dxdy \tag{5.5}$$

When receiver nonlinearity is present, this error rate will be modified using the change of variables technique. Assuming a third order polynomial model, the nonlinear probability of

symbol error will be:

$$P(\text{error}|s_k) = 1 - \int_{c_2}^{c_3}\int_{c_1}^{c_2} \frac{1}{\pi N_0} \frac{1}{|\alpha_1 + 3\alpha_3(g^{-1}(x'))^2||\alpha_1 + 3\alpha_3(g^{-1}(y'))^2|} * e^{-\frac{1}{N_0}((g^{-1}(x') - \Re(s_k))^2 + (g^{-1}(y') - \Im(s_k))^2)} dxdy \quad (5.6)$$

To determine the complete probability of error for the M-QAM signal, the P(error|s) for each symbol s will be summed and then divided by M. When Gray coding is used, the probability of bit error will be approximately $\frac{1}{log_2 M}$ multiplied by the symbol error. Because neighboring symbols will differ by only one bit, if a symbol is received in error the most likely scenario will be that only one of the bits is received in error.

5.2 Bit and Symbol Error Rate Expressions in the Presence of Interference

When receiver nonlinearity is present, a high powered interfering signal will desensitize the desired signal that is close in frequency to it. Using the probability density equations derived in Chapter 4, the performance loss from this blocking signal will be derived. Like in Chapter 4, the cases of a tone blocker, M-PAM modulated blocker, and M-QAM modulated blocker will be considered. The following are the assumptions made in this analysis:

- The blocking signal has the same symbol period as the signal of interest
- The blocking signal and the signal of interest are unsynchronized
- The bandwidth of the desired signal and the distortion product created by the blocking signal are equal

5.2.1 Tone Interference

A tone blocker can be modeled with the equation $i(t) = A_i \cos(2\pi f_2 t + \phi)$ with the desired signal at some frequency f_1. For an M-PAM signal of interest, the probability of error for each symbol x_k with left and right decision boundaries without the blocking signal will follow (5.2). Using a third order polynomial model, the probability of symbol error with the blocking signal becomes:

$$\mathrm{P(error|x}_k) = \frac{1}{\sqrt{\pi N_0}}\left(\int_{-\infty}^{d_l} \frac{1}{\mathrm{M}\left|\alpha_1 + \frac{3}{2}\alpha_3(A_i e^{j\phi})^2 + \frac{9}{4}\alpha_3(g^{-1}(y))^2\right|} e^{\frac{-(g^{-1}(y)-x_k)^2}{N_0}} dy + \int_{d_r}^{\infty} \frac{1}{\mathrm{M}\left|\alpha_1 + \frac{3}{2}\alpha_3(A_i e^{j\phi})^2 + \frac{9}{4}\alpha_3(g^{-1}(y))^2\right|} e^{\frac{-(g^{-1}(y)-x_k)^2}{N_0}} dy \right) \tag{5.7}$$

Therefore the total probability of symbol error becomes the sum of each of the probability of errors for each of the M symbols, divided by M. The error probability for an M-QAM signal follows the same pattern, the probability of error for one symbol s_k when a tone blocker is present will be:

$$\mathrm{P(error|s}_k) = 1 - \left(\int_{c_2}^{c_3} \int_{c_1}^{c_2} \frac{1}{\pi N_0} \frac{1}{\mathrm{M}\left|\alpha_1 + \frac{3}{2}\alpha_3(A_i e^{j\phi})^2 + \frac{9}{4}\alpha_3(g^{-1}(x'))^2\right|} * \frac{1}{\mathrm{M}\left|\alpha_1 + \frac{3}{2}\alpha_3(A_i e^{j\phi})^2 + \frac{9}{4}\alpha_3(g^{-1}(y'))^2\right|} e^{-\frac{1}{N_0}((g^{-1}(x')-\Re(s_k))^2+(g^{-1}(y')-\Im(s_k))^2)} dx dy \right) \tag{5.8}$$

with the total probability of symbol error being:

$$\mathrm{P(error)} = \frac{1}{\mathrm{M}} \sum_{k=1}^{\mathrm{M}} \mathrm{P(error|s}_k) \tag{5.9}$$

5.2.2 M-PAM Interference

An M-PAM modulated blocker will add distortion and amplitude modulation to the signal of interest. Using the same notation as Chapter 4, the probability of symbol error for each

of the M symbols in an M-PAM signal will be:

$$\mathrm{P(error|x}_k) = \sum_{m=1}^{\mathrm{M}/2} \frac{1}{\sqrt{\pi N_0}} \left(\int_{-\infty}^{d_l} \left| \frac{\partial}{\partial y} g_m^{-1}(y) \right| e^{\frac{-(g_m^{-1}(y)-x_k)^2}{N_0}} dy + \int_{d_r}^{\infty} \left| \frac{\partial}{\partial y} g_m^{-1}(y) \right| e^{\frac{-(g_m^{-1}(y)-x_k)^2}{N_0}} dy \right) \tag{5.10}$$

which integrates each of the M symbols with its decision boundaries to determine the total probability of error. The probability of error for an M-QAM signal with an M-PAM blocker will be derived in the same way, using (5.6) as the probability of error for each symbol. Therefore, the error rate for each of the M symbols in an M-QAM signal with the M-PAM blocker will be:

$$\mathrm{P(error|s}_k) = \sum_{m=1}^{\mathrm{M}/2} \left(1 - \int_{c_2}^{c_3} \int_{c_1}^{c_2} \frac{1}{\pi N_0} \left| \frac{\partial}{\partial y} g_m^{-1}(x') \right| \left| \frac{\partial}{\partial y} g_m^{-1}(y') \right| e^{-\frac{1}{N_0}((g_m^{-1}(x')-\Re(s_k))^2+(g_m^{-1}(y')-\Im(s_k))^2)} dxdy \right) \tag{5.11}$$

5.2.3 M-QAM Interference

Finally, an M-QAM blocking signal will add distortion to both the imaginary and real axes for an M-PAM and M-QAM signal of interest. The 3D pdf will be used for M-PAM to accurately account for the distortion along the imaginary axis. Therefore, the symbol error rate equation will follow the same formula for both possible signals of interest, using the $g_m(z)$ expressions for the M-QAM blocking case in Chapter 4.

$$\mathrm{P(error|s}_k) = \sum_{m=1}^{\mathrm{M}/2} \left(1 - \int_{c_2}^{c_3} \int_{c_1}^{c_2} \frac{1}{\pi N_0} \left| \frac{\partial}{\partial y} g_m^{-1}(x') \right| \left| \frac{\partial}{\partial y} g_m^{-1}(y') \right| e^{-\frac{1}{N_0}((g_m^{-1}(x')-\Re(s_k))^2+(g_m^{-1}(y')-\Im(s_k))^2)} dxdy \right) \tag{5.12}$$

This expression is identical to (5.11) except the $g_m(z)$ equations will use the complex M-QAM interference amplitudes.

5.3 Comparison of Theoretical Expressions with Simulated Results

Percent error was used to determine the accuracy of the theoretical bit error rate expressions. This error metric is defined as:

$$\text{PE} = 100\% * \left| \frac{\text{simulated} - \text{theoretical}}{\text{simulated}} \right| \tag{5.13}$$

This was calculated between the simulated and theoretical error rate values, with the error rate for the simulated case being averaged over 25 trials to smooth the simulated signal. This was calculated for the no interference case for varying modulation order PAM and QAM signals with varying amounts of nonlinearity, and then for the case of tone, M-PAM, and M-QAM interfering signals. The percent error of the no nonlinearity and no interference case was used as a basis of comparison.

5.3.1 Receiver Nonlinearity with No Interference

A simulation of an M-PAM and M-QAM transmitter and receiver was created in Matlab to measure the accuracy of the theoretical error rate expressions. Random symbols were created and modulated, and then AWGN and receiver nonlinearity was added. The error rate was then calculated for a number of trials, and the simulated and theoretical error rates were compared. Figure 5.4 shows the error rate curves for an 8-PAM signal for a linear receiver up to severe amounts of nonlinearity. As the amount of nonlinearity increases the error rate worsens, and for severe amounts around 50% of the symbols are received in error.

Visually, the simulated and theoretical plots match quite well. Figure 5.3 shows the percent error between the theoretical and simulated symbol error rates across an SNR range for the same nonlinearity range as Figure 5.4. There is no trend between the amount of nonlinearity and the percent error of the error rates, but the percent error of the linear model is similar to the nonlinear models. This shows that the error rate expressions are as accurate or better than the accepted error rate expressions for 8-PAM.

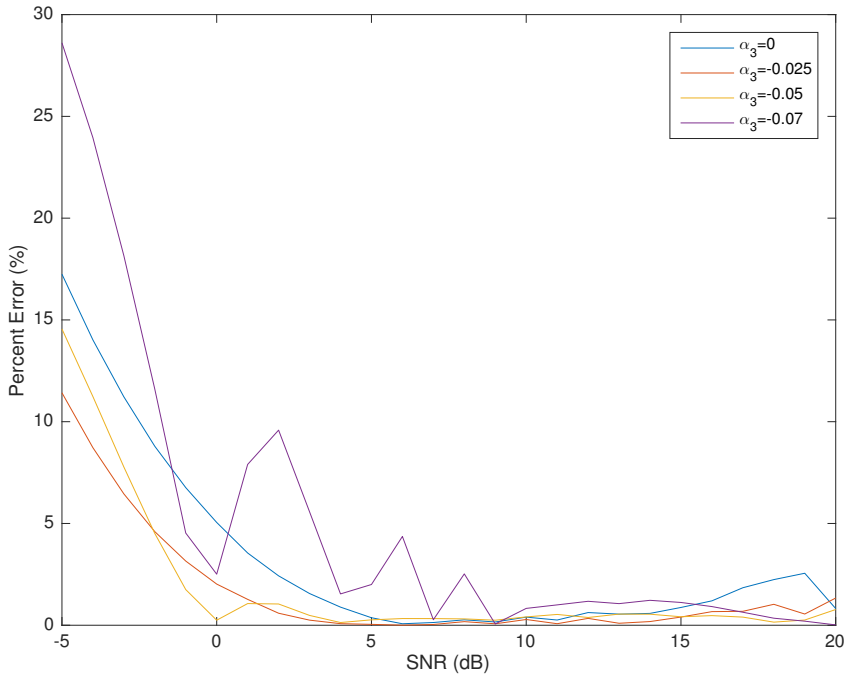

Figure 5.3: The percent error between the simulated and theoretical pdfs across SNRs from -5 to 25 dB for an 8-PAM constellation with varying amounts of receiver nonlinearity

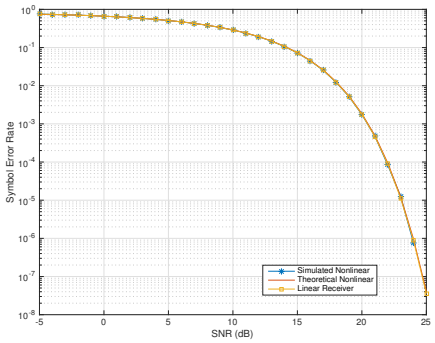

(a) Linear Receiver

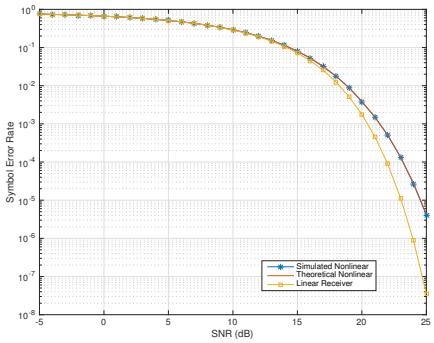

(b) Slightly Nonlinear

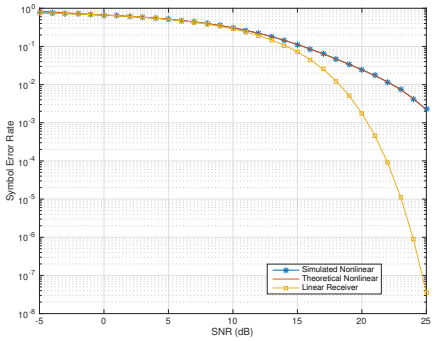

(c) Moderately Nonlinear

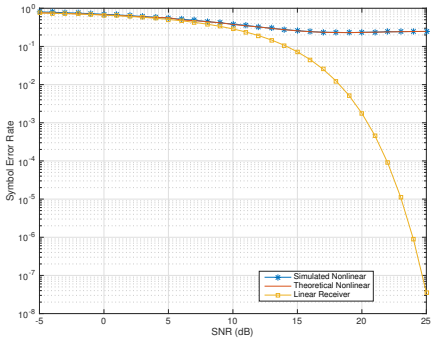

(d) Severely Nonlinear

Figure 5.4: Theoretical and simulated symbol error rates for 8-PAM with varying amounts of nonlinearity. The simulated error rate is averaged over 25 trials.

Figure 5.5 shows the symbol error rates for a 4-QAM signal with no nonlinearity and with a severe amount of nonlinearity. As the plots show, 4-QAM constellations are very resistant to nonlinearity and even severe amounts lead to little effect on the resulting symbol error rate. This is expected because the power of each of the symbols is the same. While the nonlinearity changes the distribution of the symbols as shown in Figure 5.6, having only one

power level in the constellation causes each symbol to be affected in the same way, preventing the symbols from shifting into the decision regions of the neighboring symbols.

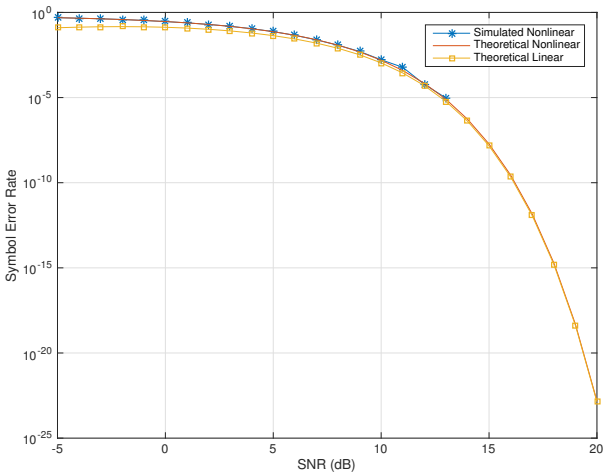

(a) The symbol error rate for linear receiver

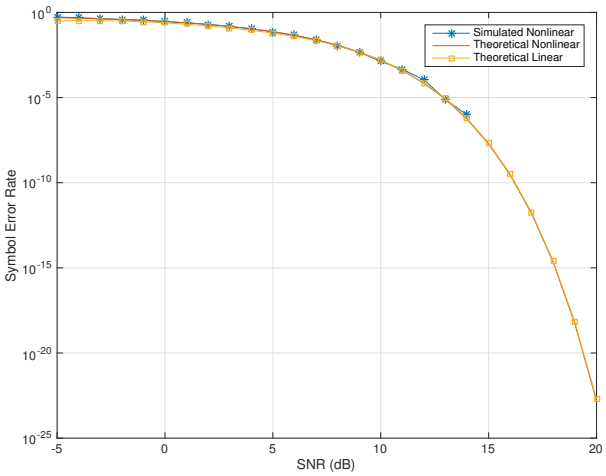

(b) The symbol error rate for $\alpha_1 = 1$ and $\alpha_3 = -0.1$

Figure 5.5: The symbol error rate of a 4-QAM signal with no nonlinearity and with a severe amount of receiver nonlinearity.

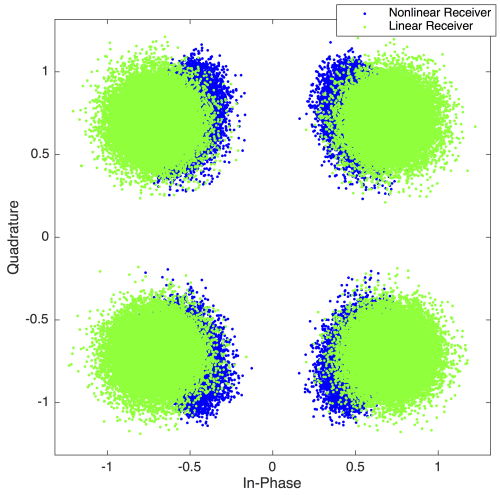

Figure 5.6: The signal constellation of a 4-QAM signal with and without receiver nonlinearity at an SNR of 15 dB, $\alpha_1 = 1$ and $\alpha_3 = -0.1$

5.3.2 Receiver Nonlinearity with Interference

5.3.2.1 Tone Blocking Signal

Figure 5.7 shows the theoretical and simulated symbol error rates of a 4-PAM signal with a tone blocker of varying amplitude. As the power of the blocking signal increases, the error rate of the 4-PAM signal approaches 0.5, showing that the interfering signal has completely blocked any information from being transmitted. Figure 5.8 shows the percent error of the symbol error rates across SNRs from -5 to 20 dB with the same blocker power levels as in Figure 5.7. At SNRs below 5 dB, the percent error was greater than 10%, but at higher SNRs the percent error was mainly less than 5% for all of the blocking amplitudes tested.

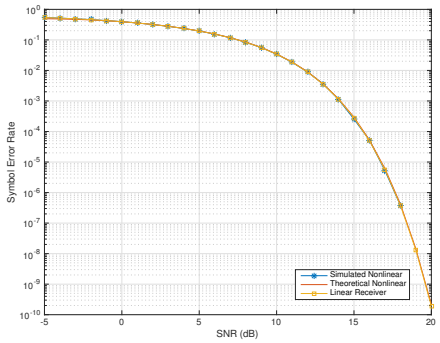

(a) No nonlinearity, no interference

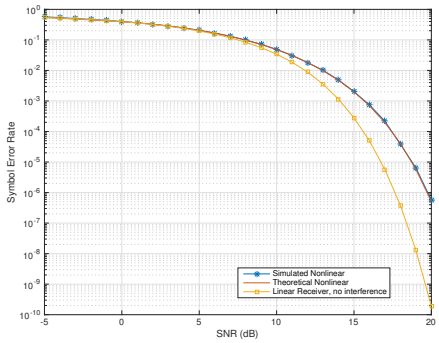

(b) $A_i = 0.4 * E_{av}$

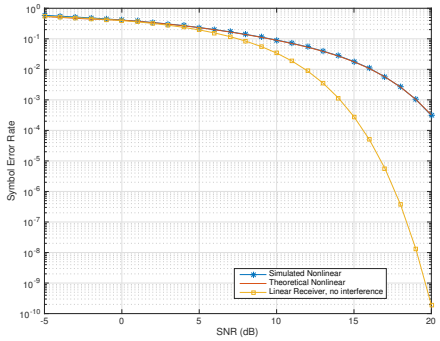

(c) $A_i = 0.6 * E_{av}$

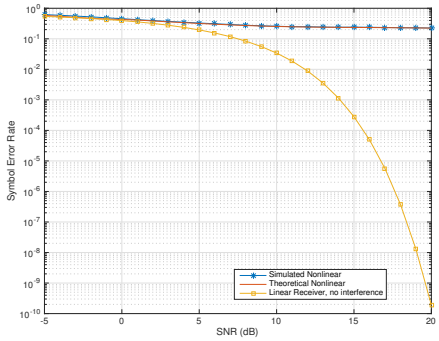

(d) $A_i = 0.8 * E_{av}$

Figure 5.7: Theoretical and simulated symbol error rates for 4-PAM with receiver nonlinearity and tone interference of varying amplitudes. E_{av} is the average energy of the 4-PAM signal.

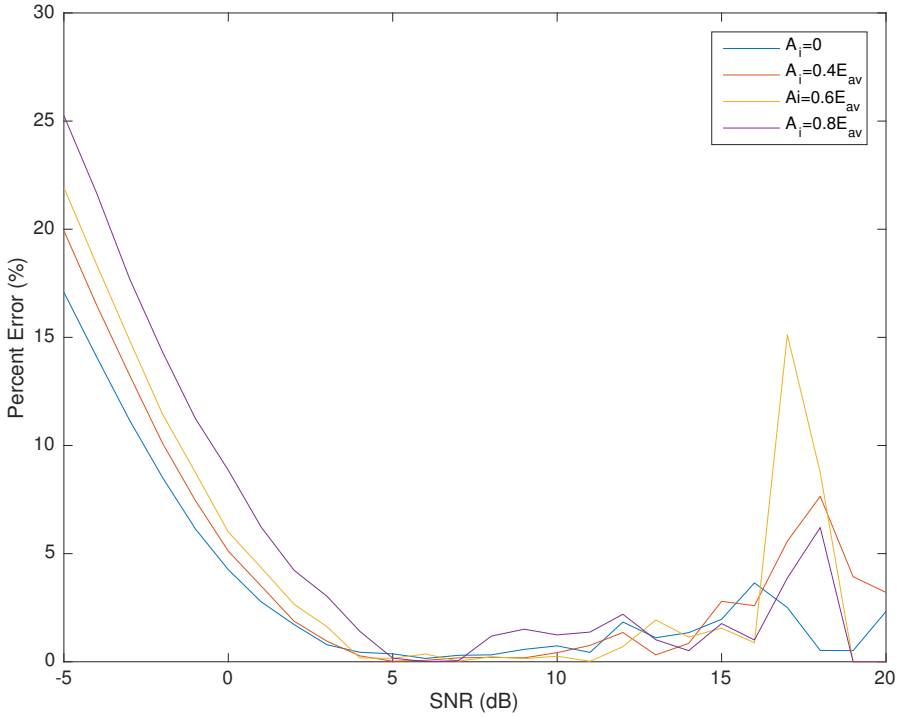

Figure 5.8: The percent error of the symbol error rate of a 4-PAM signal with 4-PAM blocking signal of varying amplitude

5.3.2.2 M-PAM Blocking Signal

Figure 5.9 shows the theoretical and simulated symbol error rate curves for a 4-PAM signal of interest with a 4-PAM blocking signal with varying average signal energy. Like the tone blocker case, the simulated and theoretical plots line up very well, with slight inaccuracies at SNRs below 0 dB. This effect is because the simulated pdf at low SNRs will not have as smooth of a curve as the higher SNRs for the same number of iterations of the simulation. Figure 5.10 shows the percent error for each of the blocking signals tested. The error rate

expressions for the presence of the blocking signal have similar accuracies to the error rate expression for the linear receiver case.

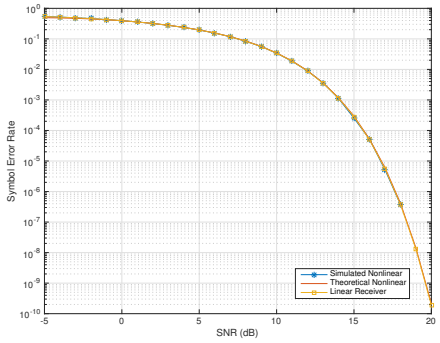

(a) No nonlinearity, no interference

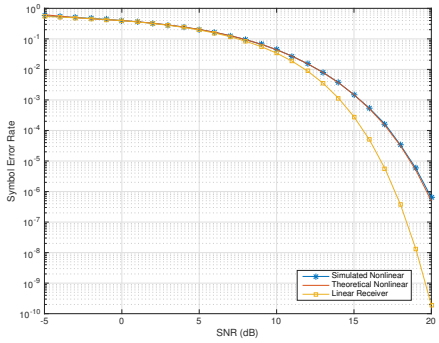

(b) $E_{av_i} = 0.5E_{av_s}$

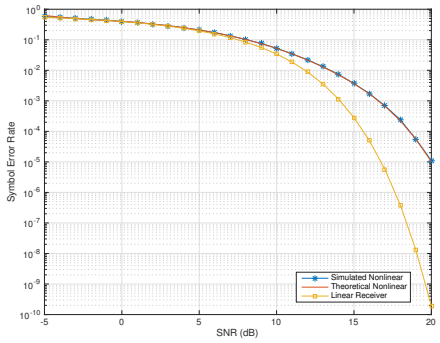

(c) $E_{av_i} = 0.75E_{av_s}$

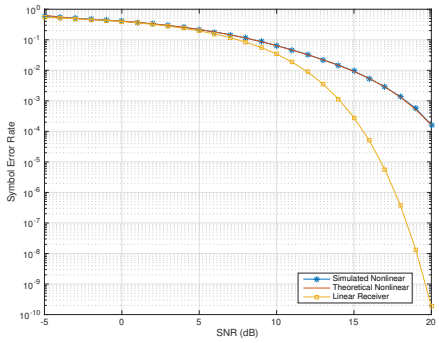

(d) $E_{av_i} = E_{av_s}$

Figure 5.9: Theoretical and simulated symbol error rates for 4-PAM with receiver nonlinearity and 4-PAM interference of varying average energy.

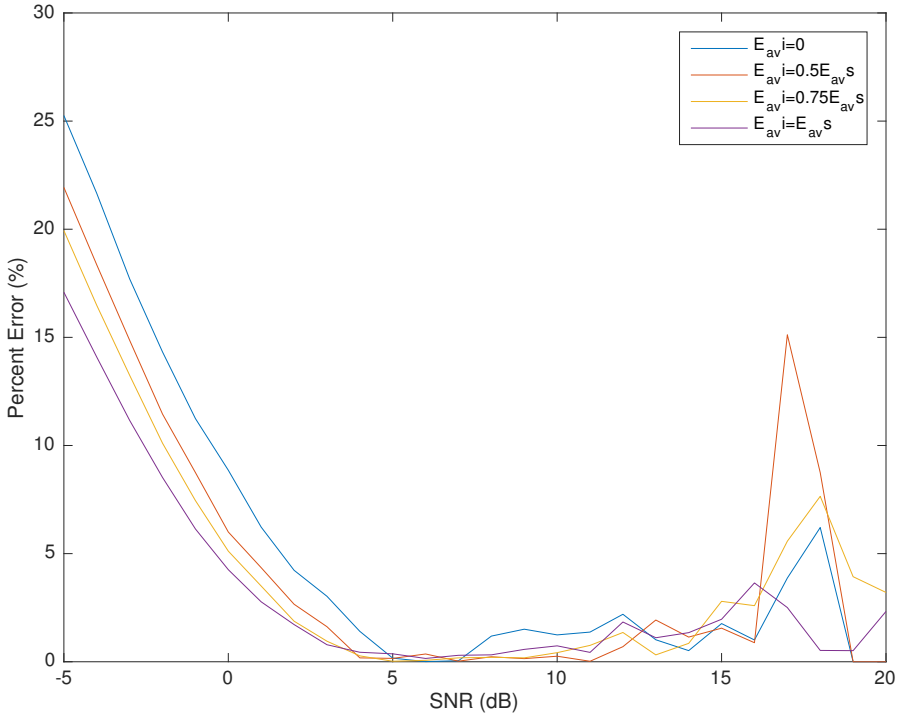

Figure 5.10: The percent error of the symbol error rate of a 4-PAM signal with a tone blocking signal of varying amplitude

5.3.2.3 M-QAM Blocking Signal

Like the 2-PAM and 4-QAM cases, the bit and symbol error rate of a 2-PAM signal with a 4-QAM blocker will be more resistant to blocking signals than a higher order PAM signal of interest. Figure 5.11 shows the signal constellation of a 2-PAM signal with a large amount of receiver nonlinearity and a blocking signal. Even though the signal is very distorted by the interference, the received signal points do not move much closer to the decision boundary at 0, and therefore the error rate will only be minimally affected as shown in Figure 5.12.

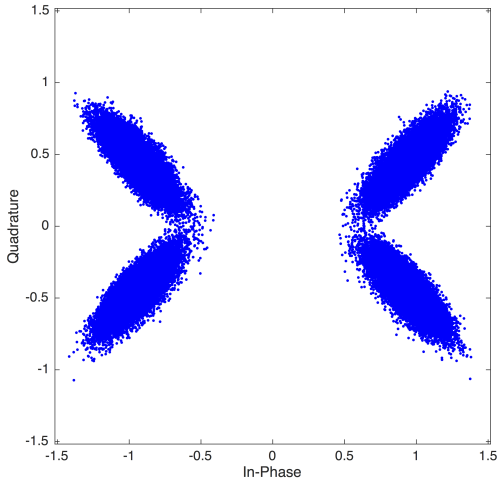

Figure 5.11: The simulated signal constellation of a simulated 2-PAM signal with a 4-QAM blocker, $\alpha_1 = 1$, $\alpha_3 = -0.05$, and $A_i = \sqrt{3}$

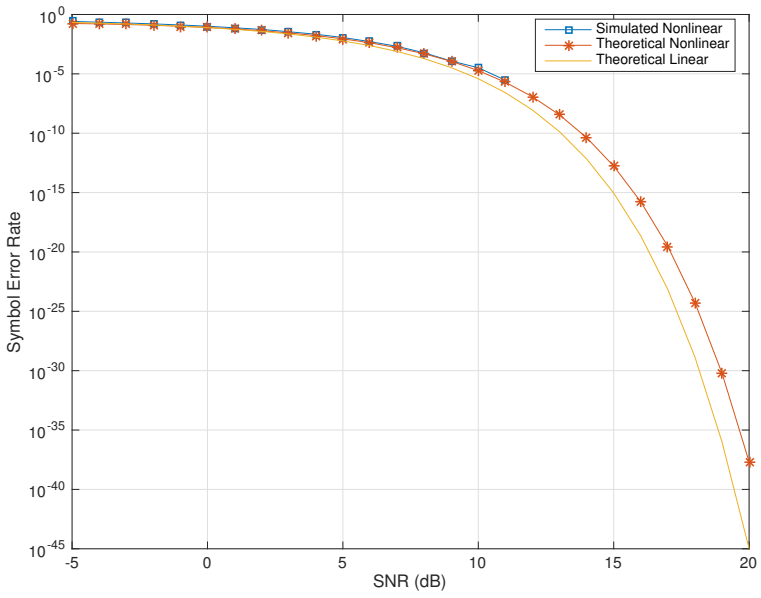

Figure 5.12: The symbol error rate for a simulated 2-PAM signal with 4-QAM interference, $\alpha_1 = 1$, $\alpha_3 = -0.05$, and $A_i = \sqrt{3}$

5.4 The Effect of the Phase Offset on Performance

While the performance curves in Section 5.3 were generated for a 0° phase shift between the blocker and the signal of interest, the phase offset can lead to a large variation in performance. For example, Figure 5.13 shows a comparison of the performance of a 4-PAM blocker on a 4-PAM signal when the phase offset is 0° and when it is 45°. Because the effect of the phase offset is squared, the phase offset of 45° will cause a 90° phase shift in the interfering term that is added to the signal of interest, leading to mainly vertical distortion in the received signal constellation. In contrast, the blocker with a 0° phase shift will add distortion in the horizontal direction to the signal of interest, shifting the received symbols towards each other. This 45° difference in phase leads to a large 4 dB difference in performance. The blocker with the 45° phase offset leads to almost no increase in the error rate compared to the linear receiver case. Figure 5.14 shows a comparison between these two signal constellations caused by the difference in phase offset. The 45° phase offset leads to vertical distortion and rotation in the symbols while the 0° phase offset leads to horizontal distortion. This example shows that when the blocking signal and the signal of interest are unsynchronized, there can be large performance differences depending on how the two signals combine at the receiver.

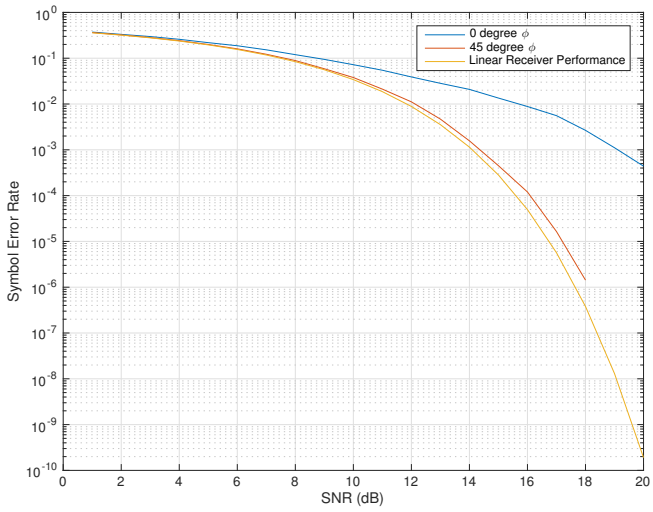

Figure 5.13: The simulated symbol error rate for a 4-PAM signal with 4-PAM interference with two ϕ values.

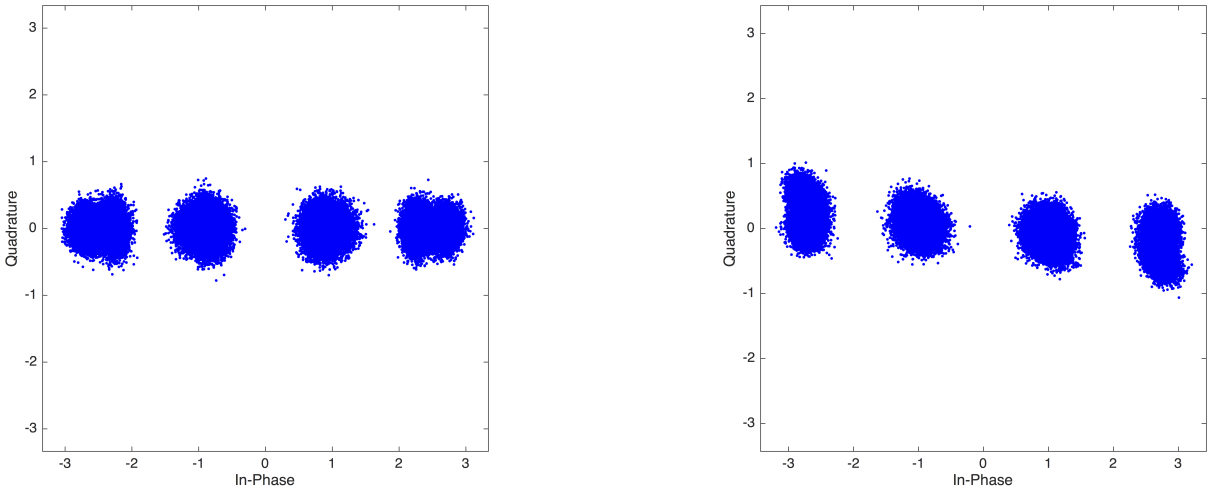

(a) Phase offset of 0°

(b) Phase offset of 45°

Figure 5.14: The received signal constellation of a 4-PAM signal with a 4-PAM blocker with two phase offset values

5.5 The Effectiveness of Blocking Signal Type on Performance

The effectiveness of the blocking signal on increasing the error rate of the signal of interest depends on the modulation type of both the blocking signal and the signal of interest. The purpose of this section is to find which type of blocking signal most significantly impacts the performance of 2-PAM, 4-PAM, 8-PAM, and 4-QAM signals of interest. These signals could be interference or intentional jamming signals. For this case, the amount of nonlinearity was held constant at $\alpha_1 = 1$ and $\alpha_3 = -0.07$, there was zero phase offset, and the average power of the blocking signals was constant for each modulation type tested. 2-PAM, 4-PAM, 8-PAM, 4-QAM, and tone blocking signals were evaluated at SNRs between -5 and 20 dB. Figure 5.15 shows the symbol error rate plots of these combinations of blocking signals and signals of interest. For the PAM modulated signals of interest, 4-QAM with a phase offset of 0 was the least effective in all three cases. 4-PAM was the most effective blocker against 2-PAM and 4-PAM while 2-PAM and the tone blocker were most effective against 8-PAM. For the 4-QAM signal of interest, 8-PAM was the most effective while the tone and 2-PAM blockers were the least effective. [43] found that 2-PAM (BPSK) was the most optimal jamming signal for 2-PAM and 4-PAM signals of interest which agrees with these results because a 4-PAM blocker has the effect of a 2-PAM jammer at the frequency of interest. While all combinations of blocker types and signal types could not be tested, these results show that PAM blockers tend to have the largest detrimental effect on PAM signals of interest and

2-PAM blockers have little effect on QAM signals of interest.

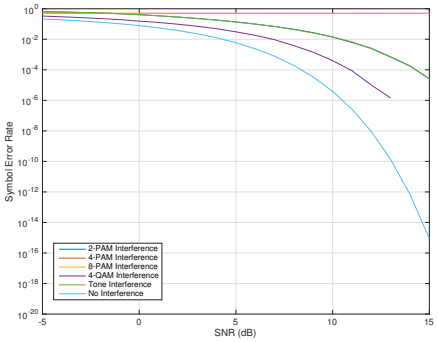

(a) 2-PAM Signal of Interest

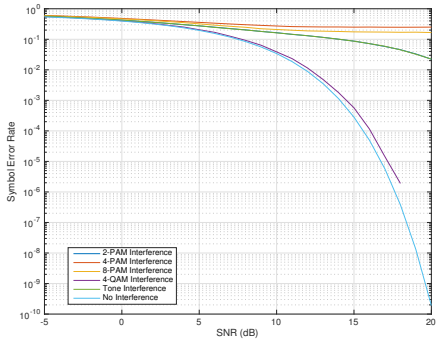

(b) 4-PAM Signal of Interest

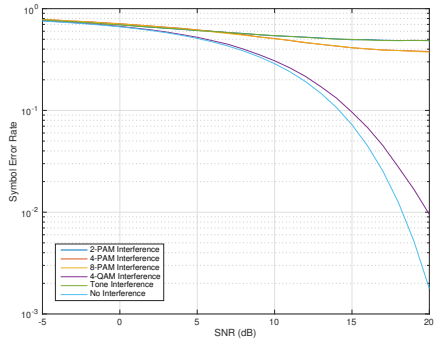

(c) 8-PAM Signal of Interest

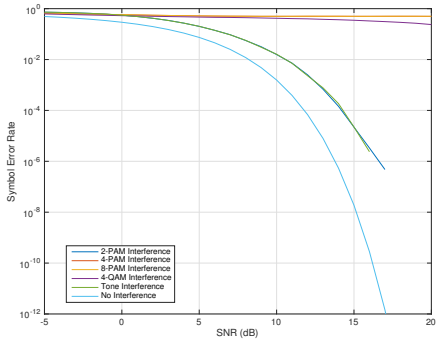

(d) 4-QAM Signal of Interest

Figure 5.15: The simulated symbol error rates of the different blocking signals on 2-PAM, 4-PAM, 8-PAM, and 4-QAM signals of interest.

5.6 Summary

In this chapter, theoretical symbol error rates were derived for M-PAM and M-QAM signals of interest for the case of general receiver nonlinearity, and for the case where the nonlinearity

has caused distortion from strong adjacent signals. The accuracy of the derived expressions was demonstrated with a percent error calculation, which showed that the accuracy of these expressions was similar to the accuracy for existing expressions for a linear receiver at SNRs greater than 5 dB. Additionally, it was shown that the phase offset between the blocking signal and the signal of interest can lead to large performance differences depending on how the phase offset shifts the received symbols of the signal. Finally, the type of blocking signal had a large performance impact on the signal of interest. 4-QAM modulated blockers had a small impact on the performance of PAM signals of interest, while 2-PAM modulated blockers had little impact on 4-QAM signals of interest.

Chapter 6

Conclusions

As the RF spectrum becomes more crowded, measuring and mitigating the effects of receiver nonlinearity will become essential. Not only does nonlinearity add amplitude and phase distortion to a received signal, signals in adjacent channels can block and add modulation to the signal of interest. Because nonlinear receivers are less costly than linear receivers, having performance equations that take the nonlinearity into account can allow for finding the maximum amount of nonlinearity that still meets a specific performance requirement. This thesis examined how to quantitatively evaluate the impact of these nonlinear effects on the probability density functions and bit and symbol error rates of amplitude modulated signals. Three aspects of the impact of nonlinearity on performance were discussed.

First, the impact of receiver nonlinearity on the probability density functions of M-PAM and M-QAM signals was analyzed. Using a memoryless polynomial model to model the nonlinearity allows for change of variables to be used to derive theoretical pdfs that take the

nonlinearity into account. Matlab simulations of M-PAM and M-QAM signals across a range of SNRs and degrees of nonlinearity showed that these new expressions have very similar accuracy to the accepted pdf expressions for linear receivers used elsewhere in related works. At low SNRs, these expressions were slightly less accurate as the amount of nonlinearity increased, which is most likely due to using a histogram function to create the simulated pdf. This effect could possibly be mitigated by using a different method to create the simulated pdf and a different statistical method to measure the error between the simulated and theoretical pdfs.

Second, the impact of adjacent blocking signals that desensitize the signal of interest on the pdfs of M-PAM and M-QAM signals was examined. Theoretical pdfs were derived for the cases of tone blockers, M-PAM modulated blockers, and M-QAM modulated blockers that had some degree of phase offset from the signal of interest. These expressions were just as accurate as the expressions for a linear receiver for the case where the signal of interest was M-PAM modulated and were slightly less accurate along the imaginary axis for an M-QAM signal of interest. While assuming that an M-QAM signal is a combination of two independent $\sqrt{\mathrm{M}}$-PAM signals is accurate for the linear receiver case, this assumption might not completely hold for the nonlinear receiver case. However, the theoretical pdf still provides a close approximation to the actual pdf.

Finally, these pdf expressions were integrated at the decision boundaries to find bit and symbol error rate expressions for nonlinear receivers with and without blocking signals. Like the pdf accuracy measurements, the accuracy was slightly lower at low SNRs for high re-

ceiver nonlinearity, but was highly accurate at SNRs greater than 5-10 dB depending on the type of the signal of interest. For the blocking signal scenarios, the accuracy followed the same pattern for M-PAM signals of interest, but was slightly less accurate when they were M-QAM modulated. A possible reason for this difference is simulation error when calculating the inverses for a complex signal of interest. Additionally, the phase offset between the blocking signal and the signal of interest was found to produce a large impact on the resulting performance, as well as the type of blocking signal due to the direction in which the distortions occur. Finally, M-QAM modulated blocking signals tended to have a small impact on M-PAM signals of interest and 2-PAM blocking signals had a small impact on QAM signals of interest.

For future work, some of the assumptions made in Chapters 4 and 5 should be relaxed for more accurate analysis of real world scenarios. Because a partial bandwidth overlap between the distortion product and the signal of interest will decrease performance, but not as much as a full overlap, the analysis should be extended to measure this effect. Some receivers have significant memory effects so additionally the analysis should be extended for a receiver model with memory. The Hammerstein model adds an FIR filter before a memoryless polynomial to simulate these effects and this filter could be incorporated into the derived pdf and error rate equations.

To extend this work, a software-defined radio testbed instead of Matlab simulation will be used to measure the accuracy of the expressions derived in this work. This would allow for a more realistic system scenario. Additionally, these expressions will be derived for more

realistic channel models such as a fading model or a path loss model, using the approach reported in this thesis. One possible extension of this work would be to develop a forward error correction method for nonlinear receivers that takes into consideration that the higher powered symbol points are more likely to be received incorrectly than the lower powered points. Another extension would be a nonlinearity mitigation scheme that incorporates machine learning to find the optimal decision boundaries for varying amounts of receiver nonlinearity.

Bibliography

[1] L. Davies and P. Winter, "OFCOM: Study of current and future receiver performance," 2010. [Online]. Available: `https://www.ofcom.org.uk/__data/assets/pdf_file/0015/31911/receiver.pdf`. [Accessed: June 12, 2018].

[2] B. Razavi, *RF Microelectronics*, 2nd ed. Prentice Hall, 2011.

[3] Z. El-Khatib, L. MacEachern, and S. Mahmoud, "Modulation Schemes Effect on RF Power Amplifier Nonlinearity and RFPA Linearization Techniques," in *Distributed CMOS Bidirectional Amplfiers*, New York:Springer, 2012, pp. 7-28.

[4] H. Bouhadda, H. Shaiek, D. Roviras, R. Zayani, Y. Medjahdi, and R. Bouallegue, "Theoretical analysis of BER performance of nonlinearly amplified FBMC/OQAM and OFDM signals," *EURASIP Journal on Advances in Signal Processing*, 2014:60, 2014.

[5] F. Edalat, "Effect of Power Amplifier Nonlinearity on System Performance Metric, Bit-Error-Rate (BER)," M.S. thesis, Massachusetts Institute of Technology, 2003.

[6] S. Merchan, A. Armada, J. Garcia, "OFDM performance in amplifier nonlinearity," *IEEE Transactions on Broadcasting*, vol. 44, issue 1, pp. 106-114, March 1998.

[7] T. Schenk, *RF Imperfections in High-rate Wireless Systems: Impact and Digital Compensation*, Dordrecht, The Netherlands: Springer, 2008.

[8] C. van den Bos, M. Kouwenhoven, W. Serdijn, "Effect of Smooth Nonlinear Distortion on OFDM Symbol Error Rate," *IEEE Transactions on Communications*, vol. 49, issue 9, pp. 1510-1514, Sept. 2001.

[9] A. Singh, H. Kaur, "Non Linearity Analysis of High Power Amplifier in OFDM System," *International Journal of Computer Applications*, vol. 37, no. 2, pp. 37-41, Jan. 2012.

[10] D. Dardari, V. Tralli, A. Vaccari, "A Theoretical Characterization of Nonlinear Distortion Effects in OFDM Systems," *IEEE Transactions on Communications*, vol. 48, no. 10, pp. 1755-1764, Oct. 2000.

[11] M. Asim, D. McLernon, and M. Ghogho, "Receiver Design for OFDM in the Presence of I/Q Imbalance and Amplifier Nonlinearity," *Sensor Signal Processing for Defense*, 2012.

[12] T. Helaly, R. Dansereau, and M. El-Tanany, "Analysis of BER Performance in Presence of Nonlinear Distortion Due to PD-HPA in Downlink DS-CDMA Signals," *IEEE Communications Letters*, vol. 14, no. 4, pp. 273-275, April 2010.

[13] A. Padaki, "Fundamentals of Efficient Spectrum Access and Co-Existence with Receiver Nonlinearity," PhD Dissertation, Virginia Tech, Dec. 2017.

[14] A. Padaki, R. Tandon, and J. Reed, "Efficient Spectrum Sharing with RF Diversity: Adapting to Nonlinearity of Front Ends," *IEEE GLOBECOM*, 2015.

[15] P. Xue, H. Yang, Z. Xu, C. Zhou, and S. Zhou, "Effect of Nonlinearities in Wireless Communication with Digital Receiver," *IEEE Wireless Communications and Networking Conference*, 2013.

[16] F. Belvèze and P. Baudin, "Specifying Receiver IP2 and IP3 Based Tolerance to Modulated Blockers," *IEEE Transactions on Communications*, vol. 56, no. 10, pp. 1677-1682, Oct. 2008.

[17] J. Dsouza, "Analysis of RF Front-End Non-linearity on Symbol Error Rate in the Presence of M-PSK Blocking Signals," M.S. thesis, Virginia Tech, Blacksburg VA, July 2017.

[18] Q. Zou, M. Mikhemar, A. Sayed, "Digital Compensation of Cross-Modulation Distortion in Software-Defined Radios," *IEEE Journal of Selected Topics in Signal Processing*, vol. 3, issue 3, pp. 348-361, June 2009.

[19] E. Keehr and A. Hajimiri, "Equalization of Third-Order Intermodulation Products in Wideband Direct Conversion Receivers," *IEEE Journal of Solid-State Circuits*, vol. 43, no. 12, pp. 2853-2867, Dec. 2008.

[20] E. Keehr and A. Hajimiri, "Successive Regeneration and Adaptive Cancellation of Higher Order Intermodulation Products in RF Receivers," *IEEE Transactions on Microwave Theory and Techniques*, vol. 59, no. 5, pp. 1379-1396, May 2011.

[21] W. Zhao, H. Ma, H. Zhang, J. Jin, G. Dai, and L. Hu, "A Nonlinearity Mitigation Method for a Broadband RF Front-End in a Sensor Based on Best Delay Searching," *Sensors*, Sept. 2017.

[22] E. Rebeiz, A. Shahed Hagh Ghadam, M. Valkama, and D. Cabric, "Spectrum Sensing Under RF Non-Linearities: Performance Analysis and DSP-Enhanced Receivers," *IEEE Transactions on Signal Processing*, vol. 63, no. 8, pp. 1950-1964, April 2015.

[23] M. Grimm, M. Allén, J. Marttila, M. Valkama, and R. Thomä, "Joint Mitigation of Nonlinear RF and Baseband Distortions in Wideband Direct-Conversion Receivers," *IEEE Transactions on Microwave Theory and Techniques* vol. 62, no. 1, pp. 166-182, Jan. 2014.

[24] M. Rajashekharaiah, "Gain Control and Linearity Improvement for Low Noise Amplifiers in 5 GHz Direct Conversion Receivers," M.S. Thesis, Washington State University, May 2005.

[25] D. Mahrof, E. Klumperink, J. Haartsen, and B. Nauta, "On the Effect of Spectral Location of Interferers on Linearity Requirements for Wideband Cognitive Radio Receivers," *IEEE Symposium on New Frontiers in Dynamic Spectrum*, April 2010.

[26] M. Marcus, "Harmful Interference and Its Role in Spectrum Policy," *Proceedings of the IEEE*, vol. 102, no. 3, pp. 265-269, 2014.

[27] G. Malhotra and J. Kamali, "BER Analysis of High Speed Links with Nonlinearity," in *Asilomar Conference on Signals, Systems, and Computers.*, Nov. 2015.

[28] A. Emira, A. Valdes-Garcia, B. Xia, A. Mohieldin, A. Valero-Lopez, S. Moon, C. Xin, and E. Sanchez-Sinencio, "Chameleon: A Dual-Mode Bluetooth/WiFi Receiver Design," [Online]. Available: http://ewh.ieee.org/soc/cas/dallas/documents/ChameleonPresentation-CAS-Dallas.pdf. [Accessed: May 28, 2018].

[29] J. Vuolevi, "Analysis, Measurement, and Cancellation of the Bandwidth and Amplitude Dependence of Intermodulation Distortion in RF Power Amplifiers," PhD Dissertation, University of Oulu, 2001.

[30] M. Treml, C. Wagner, A. Stelzer, and H. Jäger, "Characterization and Modeling of Nonlinear Mixer Behavior for 77-GHz Radar Systems," *Microwave and Optical Technology Letters*, vol. 52, no. 3, pp. 639-642, March 2010.

[31] G. Zhou, H. Qian, L. Ding, and R. Raich, "On the Baseband Representation of a Bandpass Nonlinearity," *IEEE Transactions on Signal Processing*, vol. 53, no. 8, pp. 2953-2957, Aug. 2005.

[32] E. Sinkevich, and V. Mordachev, "Characterization of Radio Receiver's Front-End Nonlinearity by Measurement of Spurious-Free Dynamic Ranges," *International Symposium on Electromagnetic Compatibility*, Sept. 2012.

[33] P. Mota, J. Machado da Silva, and J. Long, "Estimation and adaptive correction of PA's nonlinearities," *13th International Mixed Signals Testing Workshop and 3rd GHz/Gbps Test Workshop*, 2007.

[34] C. Fernandes, J. Mota, and G. Favier, "Analysis and Power Diversity-Based Cancellation of Nonlinear Distortions in OFDM Systems," in *IEEE Transactions on Signal Processing*, vol. 60, issue 7, pp. 3520-3531, July 2012.

[35] J. Pedro and B. Carvalho, *Intermodulation Distortion in Microwave and Wireless Circuits*, Norwood, MA: Artech House Publishers, 2003.

[36] H. Wang, G. Li, and P. Liu, "Characterization of Third-Order Nonlinearity in Low Noise Amplifier," *IEEE Electrical Design of Advanced Packaging and Systems Symposium*, Dec. 2011.

[37] V. M, R. Paily, and A. Mahanta, "Gain, NF and IIP3 Budgeting of LTE Receiver Front End," *26th International Conference on VLSI Design and the 12th International Conference on Embedded Systems*, Jan. 2013.

[38] C. Liu and M. Damgaard, "IP2 and IP3 Nonlinearity Specifications for 3G/WCDMA Receivers," *High Frequency Electronics*, pp. 16-29, June 2009.

[39] J. Proakis and M. Salehi, *Digital Communications*, 5th ed. McGraw-Hill, 2008.

[40] N. McMullen, D. Ochoa, "Non-Monotonic Transformations of Random Variables," Dec. 2016. [Online]. Available: http://cknudson.com/StudentWork/Transforms.pdf. [Accessed: June 28, 2018].

[41] R. Meyer and A. Wong, "Blocking and Desensitization in RF Amplifiers," *IEEE Journal of Solid-State Circuits*, vol. 30, no. 8, pp. 944-946, Aug. 1995.

[42] G. Stüber, "Principles of Mobile Communication," 2nd Ed. Kluwer Academic Publishers, 2017, pp. 471-473.

[43] S. Amuru, R. M. Buehrer, "Optimal Jamming against Digital Modulation," *IEEE Transactions on Information Forensics and Security*, vol. 10, issue 10, pp. 2212-2224, Oct. 2015.